The Astrophysical Journal Supplement Series, 227:30 (19pp), 2016 December doi:10.3847/1538-4365/227/2/30

THE PALOMAR TRANSIENT FACTORY AND RR LYRAE: THE METALLICITY–LIGHT CURVE RELATION BASED ON AB-TYPE RR LYRAE IN THE *KEPLER* FIELD

Chow-Choong Ngeow[1], Po-Chieh Yu[1], Eric Bellm[2], Ting-Chang Yang[1], Chan-Kao Chang[1], Adam Miller[3,4,6], Russ Laher[5], Jason Surace[5], and Wing-Huen Ip[1]
[1] Graduate Institute of Astronomy, National Central University, Jhongli 32001, Taiwan; cngeow@astro.ncu.edu.tw
[2] Cahill Center for Astronomy and Astrophysics, California Institute of Technology, Pasadena, CA 91125, USA
[3] Division of Physics, Mathematics, and Astronomy, California Institute of Technology, Pasadena, CA 91125, USA
[4] Jet Propulsion Laboratory, California Institute of Technology, Pasadena, CA 9110, USA
[5] Spitzer Science Center, California Institute of Technology, Pasadena, CA 91125, USA
Received 2016 August 19; revised 2016 October 11; accepted 2016 October 27; published 2016 December 15

ABSTRACT

The wide-field synoptic sky surveys, known as the Palomar Transient Factory (PTF) and the intermediate Palomar Transient Factory (iPTF), will accumulate a large number of known and new RR Lyrae. These RR Lyrae are good tracers to study the substructure of the Galactic halo if their distance, metallicity, and galactocentric velocity can be measured. Candidates of halo RR Lyrae can be identified from their distance and metallicity before requesting spectroscopic observations for confirmation. This is because both quantities can be obtained via their photometric light curves, because the absolute *V*-band magnitude for RR Lyrae is correlated with metallicity, and the metallicity can be estimated using a metallicity–light curve relation. To fully utilize the PTF and iPTF light-curve data in related future work, it is necessary to derive the metallicity–light curve relation in the native PTF/iPTF *R*-band photometric system. In this work, we derived such a relation using the known ab-type RR Lyrae located in the *Kepler* field, and it is found to be $[Fe/H]_{PTF} = -4.089–7.346P + 1.280\phi_{31}$ (where P is pulsational period and ϕ_{31} is one of the Fourier parameters describing the shape of the light curve), with a dispersion of 0.118 dex. We tested our metallicity–light curve relation with new spectroscopic observations of a few RR Lyrae in the *Kepler* field, as well as several data sets available in the literature. Our tests demonstrated that the derived metallicity–light curve relation could be used to estimate metallicities for the majority of the RR Lyrae, which are in agreement with the published values.

Key words: distance scale – stars: abundances – stars: variables: RR Lyrae

1. INTRODUCTION

The Palomar Transient Factory (PTF, 2009–2012, see Law et al. 2009; Rau et al. 2009) and its successor, the intermediate Palomar Transient Factory (iPTF, 2013–2016),[7] are dedicated wide-field synoptic sky survey projects with aims of detecting various types of transients in the universe. Given the synoptic nature of PTF/iPTF surveys, a large number of known or new RR Lyrae with homogeneous light-curve data is expected to be found in PTF/iPTF data. Since RR Lyrae are population II standard candles at which they have roughly a constant absolute magnitude in *V* band (M_V), RR Lyrae have been used in various distance-scale studies such as tracing the Galactic halo structure (for example, see Watkins et al. 2009; Sesar et al. 2010). Therefore, we have initiated a program to investigate the properties of RR Lyrae in the PTF/iPTF native *R*-band photometric system (hereafter R_{PTF}).

It is well-known that M_V for RR Lyrae is correlated with metallicity (for example, see McNamara 1999; Caputo et al. 2000; Demarque et al. 2000; Sandage & Tammann 2006), where the metallicity is mostly measured or expressed in terms of [Fe/H], then the distance to an RR Lyrae can be deduced by knowing its metallicity and hence its M_V value.[8] The best way to obtain [Fe/H] is via a spectroscopic technique; however, this can be quite expensive in terms of telescope time. Fortunately, photometric [Fe/H] for RR Lyrae can be estimated via the metallicity–light curve relation, at which the light curves for RR Lyrae can be fitted with a truncated sine-series of Fourier decomposition (for example, see Simon & Lee 1981; Deb & Singh 2009)[9]:

$$m(t) = m_0 + \sum_{i=1}^{n} A_i \sin\left(\frac{2i\pi t}{P} + \phi_i\right), \quad (1)$$

where n is the order of fitting, P is pulsation period in days, and t is time of observation. The mean magnitude m_0, amplitude A_i, and phase ϕ_i values at given ith-order can be obtained by fitting the observed light-curve data with Equation (1). The light-curve parameters, or Fourier parameters, can be expressed in terms of A_i and ϕ_i:

$$R_{ij} = \frac{A_i}{A_j}; \quad \phi_{ij} = \phi_i - i\phi_j. \quad (2)$$

The metallicity–light curve relation for fundamental mode *ab*-type RR Lyrae (hereafter RRab) was first quantitatively studied in Simon (1988). Later, such a relation was derived, or fitted, from field RRab in Kovács & Zsoldos (1995), and subsequently extended by Jurcsik & Kovács (1996). In Jurcsik & Kovács (1996), such a relation is given as $[Fe/H]_V = -5.038–5.394P + 1.345\phi_{31}$, where $\phi_{31} = \phi_3 - 3\phi_1$ is calculated using Equations (1) and (2) based on the *V*-band light curves. A preliminary updated version of the Jurcsik & Kovács (1996) relation is presented in

[6] Hubble Fellow.
[7] http://www.ptf.caltech.edu/iptf
[8] Note that the application of the M_V–[Fe/H] relation to derive distance is still prone to several issues such as reddening to individual stars, the form of the M_V–[Fe/H] relation (linear, quadratic, or two relations for metal-rich and metal-poor RR Lyraes), and evolutionary effects (such as empirical diagnostics to quantify the evolution away from the zero age horizontal branch). Recent discussions on these issues can be found, for example, in Braga et al. (2015) and Marconi et al. (2015). Detailed investigations of these issues, however, are beyond the scope of this paper and will be addressed in subsequent papers. The current paper, which represents the first paper in a series, only deals with the [Fe/H] part in the M_V–[Fe/H] relation.
[9] Note that their Fourier decomposition is expressed as a cosine-series, instead of a sine-series.

Martinez-Vazquez et al. (2016), which incorporates RR Lyrae in globular clusters. Other metallicity–light curve relations based on the V-band light curves can be found, for example, in Sandage (2004). Besides the V-band light curves, Smolec (2005) gives the relation based on I-band light curves. Wu et al. (2006) and De Lee (2008) derived a similar relation as in Jurcsik & Kovács (1996) for unfiltered, or white light, CCD observations, and for the g-band SDSS (Sloan Digitized Sky Survey) data, respectively. Watkins et al. (2009), Sesar et al. (2010) and Oluseyi et al. (2012) further developed the metallicity–light curve relation in the SDSS photometric system with additional terms in the relation. Similarly, Nemec et al. (2011) and Nemec et al. (2013) derived such a relation in the *Kepler* magnitude (K_p) system. Alternatively, Deb & Singh (2010) and Skowron et al. (2016) derived the Fourier interrelations to convert the ϕ_{31} parameters in I band to V band and then applied the metallicity–light curve relations mentioned. The validity of such a metallicity–light curve relation has been tested and verified, for example, in Jurcsik (2003), Gratton et al. (2004), Kovács (2005), Wu et al. (2006), and Kunder & Chaboyer (2008).

To fully utilize the RR Lyrae found in the PTF/iPTF data for future distance-scale work, it is necessary to derive the metallicity–light curve relation in the native $R_{\rm PTF}$-band photometric system. Even though, in principle, it is possible to apply the transformation equation provided in Ofek et al. (2012a) to convert the PTF/iPTF photometry in the $g_{\rm PTF}$-band to the Johnson-Cousin V-band and hence to apply the Jurcsik & Kovács (1996) relation; in practice, this is difficult to achieve because (1) this transformation requires the $(V - R_c)$ color curves for the RR Lyrae found in PTF/iPTF to be available, but we generally do not have such data, and (2) the majority of the data taken in PTF/iPTF are in the $R_{\rm PTF}$-band. Therefore, direct derivation of the metallicity–light curve relation in the native $R_{\rm PTF}$-band is desirable. In this work, we present the derivation of such a relation by using the known RR Lyrae located in the *Kepler* field, because these RR Lyrae possess very precise and accurate period determination based on the *Kepler* light curves and spectroscopic measurements of [Fe/H] (Nemec et al. 2013). A brief description of the PTF/iPTF project is presented in Section 2. The PTF/iPTF data for RR Lyrae in the *Kepler* field were mentioned in Section 3, followed by the construction of the light curves in Section 4. Based on the PTF/iPTF light curves, we derived the ϕ_{31} Fourier parameters in Section 5. The $R_{\rm PTF}$-band metallicity–light curve relation will be derived and tested in Section 6. Finally, a discussion and our conclusions will be presented in Section 7. Throughout the paper, the Fourier parameter ϕ_{31} is based on the sine-series as shown in Equation (1), which can be converted to the cosine-based ϕ_{31} by subtracting π (that is, $\phi_{31}^{\rm cosine} = \phi_{31}^{\rm sine} - \pi$). Also, as a reminder, throughout the paper, a ± 0.25 dex difference at [Fe/H] $= -1.5$ dex corresponds to roughly a factor of two difference in metal abundance by mass.

2. BRIEF DESCRIPTION OF THE PTF/iPTF PROJECT

The PTF/iPTF project mainly utilizes the 48 inch Samuel Oschin Telescope located at the Palomar Observatory, known as the P48 Telescope, to search for transients. The P48 Telescope is equipped with a wide-field mosaic camera, which consists of eleven $2\ K \times 4\ K$ CCD[10] (Rahmer et al. 2008), for the surveys carried out by both PTF and iPTF. The pixel scale of each CCD is 1.01 arc-second per pixel, hence providing a total field of view (FOV) of ~7.26-degree^2 for a single PTF/iPTF image. Observations with the P48 Telescope were mainly done in the Mould R-band filter (i.e., the $R_{\rm PTF}$ filter), with occasional observations carried out in the $g_{\rm PTF}$ or $H\alpha$ filters. The nominal exposure time for PTF/iPTF images is 60 s, which can reach a depth of 20.5 mag in the $R_{\rm PTF}$ band (with a 3σ detection).

The PTF/iPTF imaging data from the P48 Telescope was reduced and processed with two different pipelines (Law et al. 2009). One of the pipelines, based on the image subtraction technique, is tailored for quick discovery of transients; while another pipeline, hosted at the Infrared Processing and Analysis Center (IPAC), will fully reduce the raw images and provide catalogs of all detected objects in the images. Photometric calibration of the detected objects was also included in the IPAC pipeline. Further details of the IPAC pipeline and the photometric calibration procedure can be found in Ofek et al. (2012a, 2012b), Laher et al. (2014), and Surace et al. (2015), and will not be repeated here. Since the main goals for PTF and iPTF include the detections of transients (such as supernovae) in the local universe and pursue for new discoveries with dedicated and well-designed experiments, hence the cadence carried out in PTF and iPTF varies from 90 s to a few days. Time-series data from PTF/iPTF has not only been used for the search of transients, but also in studies of other time-domain phenomena such as variable stars (for example, see van Eyken et al. 2011) and asteroids (for example, see Chang et al. 2014).

3. RR LYRAE IN THE *KEPLER* FIELD AND THE PTF/iPTF LIGHT-CURVE DATA

In total, there have been 41 RR Lyrae found in *Kepler* field, including 21 non-Blazhko RRab stars, 16 Blazhko RRab stars, and 4 first overtone c-type RR Lyrae (hereafter RRc). In this work, we excluded the 4 RRc stars, because the small number of them in the sample did not permit a meaningful statistical analysis of their metallicity–light curve relation. For the RRab stars, Tables 1 and 2 listed out their basic information and summarized the available PTF/iPTF data in the $R_{\rm PTF}$ band, respectively. Note that a portion of the PTF data on the *Kepler* field is publicly available, which belongs to the first data release[11] of the PTF data. The difference in number of catalogs between the full and publicly available data ranges from 4 (for KIC 6186029) to 79 (for KIC7988343); for the majority of them, the difference is less than 10.

Using the publicly available catalog data for 16 non-Blazhko RRab stars in *Kepler* field, Ngeow (2015) attempted to derive a preliminary metallicity–light curve relation in the $R_{\rm PTF}$ band. However, it was found that the PTF light curves for 8 of them displayed a larger scatter in their light curves. These RR Lyrae have a mean $R_{\rm PTF}$ magnitude of ~14 mag or brighter, which is close to the saturation limit of PTF data (van Eyken et al. 2011; Ofek et al. 2012a). A provisional metallicity–light curve relation based on these 8 bright RRab stars exhibited a dispersion of 0.76 dex. In contrast, the remaining 8 RRab stars, with mean $R_{\rm PTF}$ magnitudes fainter than ~14 mag, showed much tighter PTF light curves, and the dispersion of the derived metallicity–light curve relation is 0.13 dex. One finding of Ngeow (2015) is that the bright RRab stars should not be used

[10] The original CFHT 12k mosaic camera consists of 12 CCD; however, one of them is out of function.

[11] http://www.ptf.caltech.edu/page/first_data_release

Table 1
Basic Information for RR Lyrae in the *Kepler* Field[a]

KIC[b]	R.A. (J2000)	Decl. (J2000)	P [days]	t_o	$\langle Kp \rangle$	Type[c]	Other Name
7198959	19:25:27.912	+42:47:03.72	0.566788	2455278.2263	7.862	RRab-B	RR Lyr
11125706	19:00:58.774	+48:44:42.30	0.6132200	2454981.0658	11.367	RRab-B	KIC 11125706
3733346	19:08:27.228	+38:48:46.19	0.6820264	2454964.7403	12.684	RRab-NB	NR Lyr
6936115	19:10:22.250	+42:27:31.57	0.52739847	2454953.2656	12.876	RRab-NB	FN Lyr
11802860	19:00:48.000	+50:05:31.27	0.6872160	2454954.2160	13.053	RRab-NB	AW Dra
6763132	19:07:48.374	+42:17:54.67	0.5877887	2454954.0702	13.075	RRab-NB	NQ Lyr
9591503	19:33:00.912	+46:14:22.85	0.5713866	2454953.5624	13.293	RRab-NB	V894 Cyg
9947026	19:19:57.958	+46:53:21.41	0.5485905	2454953.7832	13.300	RRab-NB	V2470 Cyg
7030715	19:23:24.527	+42:31:42.34	0.68361247	2454953.8427	13.452	RRab-NB	KIC 7030715
6100702	18:50:37.730	+41:25:25.72	0.4881457	2454953.8399	13.458	RRab-NB	KIC 6100702
7021124	19:10:26.681	+42:33:37.04	0.6224925	2454965.6471	13.550	RRab-NB	KIC 7021124
10789273	19:14:03.905	+48:11:58.60	0.48027971	2455807.9302	13.770	RRab-B	V838 Cyg
10136603	19:20:18.888	+47:07:48.54	0.4337747	2455778.7060	14.066	RRab-NB	V839 Cyg
7505345	18:53:25.903	+43:09:16.45	0.4737027	2455124.7072	14.080	RRab-B	V355 Lyr
7988343	19:59:50.669	+43:42:15.52	0.5811436	2454964.6700	14.494	RRab-NB	V1510 Cyg
5559631	19:52:52.740	+40:47:35.45	0.62070001	2454975.5439	14.643	RRab-B	V783 Cyg
12155928	19:18:00.490	+50:45:17.93	0.43638507	2455120.8363	15.033	RRab-B	V1104 Cyg
4484128	19:45:39.024	+39:30:53.42	0.5478642	2454970.2834	15.363	RRab-B	V808 Cyg
6070714	19:56:22.906	+41:20:23.53	0.5340941	2454964.8067	15.370	RRab-NB	V784 Cyg
5299596	19:51:16.999	+40:26:45.20	0.5236377	2454964.5059	15.392	RRab-NB	V782 Cyg
3864443	19:40:06.963	+38:58:20.35	0.4869538	2454976.3672	15.593	RRab-B	V2178 Cyg
10136240	19:19:45.279	+47:06:04.44	0.5657781	2454964.7551	15.648	RRab-NB	V1107 Cyg
9508655	18:49:08.369	+46:11:54.96	0.5942369	2454964.7820	15.696	RRab-NB	V350 Lyr
9658012	19:41:20.004	+46:23:28.64	0.533206	2455779.9450	16.001	RRab-NB	KIC 9658012
9697825	19:01:58.634	+46:26:45.74	0.5575765	2454988.9332	16.001	RRab-B	V360 Lyr
7742534	19:10:53.403	+43:24:54.94	0.4564851	2454964.7860	16.002	RRab-NB	V368 Lyr
6183128	18:52:50.359	+41:33:49.47	0.561691	2455245.1590	16.260	RRab-B	V354 Lyr
3866709	19:42:07.997	+38:54:42.30	0.47070609	2454964.6037	16.265	RRab-NB	V715 Cyg
8344381	18:46:08.640	+44:23:13.99	0.5768288	2454964.9231	16.421	RRab-NB	V346 Lyr
9578833	19:09:40.637	+46:17:18.17	0.5270283	2455326.1915	16.537	RRab-B	V366 Lyr
7257008	18:47:27.408	+42:49:52.68	0.51177516	2455758.5859	16.542	RRab-B	KIC 7257008
7671081	19:09:36.634	+43:21:49.97	0.5046123	2454996.3226	16.653	RRab-B	V450 Lyr
9001926	18:52:01.805	+45:18:31.61	0.5568016	2455082.6820	16.914	RRab-B	V353 Lyr
9973633	19:58:49.068	+46:50:56.83	0.51075	2455780.3655	16.999	RRab-B	KIC 9973633
9717032	19:38:19.155	+46:27:47.06	0.5569092	2455779.8956	17.194	RRab-NB	KIC 9717032
6186029	18:58:25.692	+41:35:49.45	0.5131158	2455160.5957	17.401	RRab-B	V445 Lyr
7176080	18:49:24.434	+42:44:45.56	0.5070740	2454964.9588	17.433	RRab-NB	V349 Lyr

Notes.
[a] Information taken from Nemec et al. (2013).
[b] *Kepler* Input Catalog.
[c] RRab-NB: Non-Blazhko RRab stars; RRab-B: Blazhko RRab stars.

in the derivation of the metallicity–light curve relation because their photometry will be affected by saturation limits in PTF/iPTF surveys. Excluding the prototype RR Lyr (KIC 7198959) itself and V808 Cyg (KIC 4484128, because it does not have data in PTF/iPTF), there are ∼15 RRab stars (mixed of both Blazhko and non-Blazhko stars) that have mean $R_{\rm PTF}$ magnitudes brighter than ∼14 mag, which is almost half of the total 29 RRab stars that have spectroscopic [Fe/H] measurements (Nemec et al. 2013). To maximize usable RRab stars in deriving the metallicity–light curve relation, we launched a dedicated iPTF experiment to re-observe these bright RRab stars with a 10 s exposure time (so their light curves will not suffer from the saturation limit), in opposition to the nominal 60 s exposure time set in the regular PTF/iPTF surveys.

3.1. The Dedicated iPTF Experiment

A dedicated iPTF experiment was carried out in four nights from 2015 May 29–31 and June 05. PTF fields that covered most of the bright RRab stars (except the prototype RR Lyr itself because it is too bright to observe with P48 Telescope) were selected to be observed repeatedly in these nights. Each of the PTF fields were observed ∼9 to ∼15 times per night, with a cadence of ∼18 to ∼20 minutes. In contrast, these RRab stars were observed one to seven times per night during the regular PTF/iPTF surveys, with nightly cadence varying for 1 night to ∼15 nights. Except the exposure time, which was reduced to 10 s, observations and data reduction for these PTF fields within our dedicated iPTF experiment were done with the same P48 Telescope, CCD camera, $R_{\rm PTF}$-band filter, and IPAC reduction pipeline as the regular PTF/iPTF surveys. Since some of the faint RRab stars fell within the footprint of the selected PTF fields, we included them in our analysis as mentioned in the next section. The number of catalogs for all RRab stars in the *Kepler* field from our dedicated iPTF experiment was listed in the last column of Table 2. Similarly, the number of catalogs from regular PTF/iPTF surveys was given in the third column of Table 2.

Table 2
Summary of PTF/iPTF $R_{\rm PTF}$-band Observations

KIC	Observing Window[a]	N_{60s}[b]	N_{10s}[b]
7198959	2011 Mar 16 to 2014 Oct 05	51	0
11125706	2012 Aug 04 to 2014 Oct 05, iPTF	44	54
3733346	2012 Aug 04 to 2012 Aug 06	7	0
6936115	2010 May 21 to 2014 Oct 05, iPTF	79	52
11802860	2012 Aug 04 to 2014 Oct 05, iPTF	75	52
6763132	2010 May 19 to 2014 Jun 20, iPTF	60	54
9591503	2010 May 27 to 2014 Oct 05, iPTF	203	51
9947026	2012 Jul 11 to 2014 Oct 05, iPTF	52	53
7030715	2010 May 21 to 2014 Oct 05, iPTF	79	52
6100702	2010 May 19 to 2014 Jun 20, iPTF	60	54
7021124	2010 May 21 to 2014 Oct 05, iPTF	79	52
10789273	2012 Aug 04 to 2014 Oct 05, iPTF	44	53
10136603	2013 Jul 11 to 2015 Oct 05, iPTF	52	53
7505345	2011 Mar 16 to 2014 Jun 20, iPTF	50	53
7988343	2011 Mar 16 to 2014 Aug 18, iPTF	81	49
5559631	2011 Aug 06 to 2014 Oct 05	46	0
12155928	2012 Aug 04 to 2014 Oct 05, iPTF	75	52
4484128	⋯	0	0
6070714	2011 Aug 06 to 2014 Oct 05	34	0
5299596	2011 Aug 02 to 2014 Oct 05, iPTF	89	51
3864443	2011 Aug 02 to 2014 Oct 05, iPTF	47	51
10136240	2012 Jul 11 to 2014 Oct 05, iPTF	52	53
9508655	2011 Jul 11 to 2014 Jun 20	152	0
9658012	2010 May 27 to 2014 Oct 05, iPTF	204	51
9697825	2011 Jul 11 to 2014 Jun 20	152	0
7742534	2011 Mar 16 to 2014 Oct 05	80	0
6183128	2010 May 19 to 2014 Jun 20, iPTF	60	0
3866709	2011 Aug 02 to 2014 Oct 05, iPTF	47	51
8344381	2011 Mar 16 to 2014 Jun 20, iPTF	50	53
9578833	2012 Jul 11 to 2014 Oct 05, iPTF	52	53
7257008	2011 Mar 16 to 2014 Jun 20, iPTF	50	53
7671081	2011 Mar 16 to 2014 Oct 05	80	0
9001926	2011 Jul 11 to 2014 Jun 20	152	0
9973633	2011 Jul 26 to 2014 Oct 05, iPTF	46	52
9717032	2010 May 27 to 2014 Oct 05, iPTF	204	51
6186029	2010 May 19 to 2014 Jun 20, iPTF	47	54
7176080	2011 Mar 16 to 2014 Jun 20, iPTF	50	53

Notes.
[a] First and last day of PTF data with nominal 60 s exposure, including the dedicated iPTF experiment (2015 May 29 to 2015 May 31 and 2015 June 05), labeled as iPTF if applicable.
[b] N_{60s}: number of $R_{\rm PTF}$-band PTF/iPTF SExtractor catalogs with the nominal 60 s exposure; N_{10s}: number of $R_{\rm PTF}$-band PTF/iPTF SExtractor catalogs with 10 s exposure taken during the dedicated iPTF experiment.

4. LIGHT-CURVE CONSTRUCTION

Catalog data from the IPAC pipeline for RRab stars in our sample were downloaded from the PTF/IPAC data archive hosted at the NASA/IPAC Infrared Science Archive (IRSA).[12] These $R_{\rm PTF}$-band PTF/iPTF SExtractor (Bertin & Arnouts 1996) catalog data, including both of the catalogs from regular PTF/iPTF surveys (with a nominal 60 s exposure time) and the dedicated iPTF experiment as mentioned previously, were stored in FITS binary table format. A python script[13] was used to extract the $R_{\rm PTF}$-band light curves for our RRab stars. This was done by matching the detected sources in the catalogs to the input RRab stars with a match radius of two arcseconds. The heliocentric Julian date (HJD), photometric magnitude, and magnitude error of the matched sources were saved into python arrays. The PTF $R_{\rm PTF}$-band magnitudes were constructed by adding the MAG_AUTO and ZEROPOINT in PTF catalogs (for more details, see Ofek et al. 2012a).

Since none of the images involved in this work were taken under photometric conditions as defined in Ofek et al. (2012a, i.e., the corresponding flag is $PHTCALFL = 0$), the extracted "raw" light curves displayed numerous outliers. The left panel of Figure 1 presents examples of the "raw" light curve for a bright and faint non-Blazhko RR Lyrae. For the 10 s light curves, plots in the left panels of Figure 1 show that one (or two) night from the dedicated iPTF experiment might be affected by weather. Furthermore, the upper-left panel of Figure 1 displayed a vertical shift between the light curves taken with the 10 s and 60 s exposure time for the bright RR Lyrae. As discussed in Ngeow (2015), the 60 s data was affected by saturation, hence some fluxes were lost when using the aperture photometry. In contrast, the faint RR Lyrae shown in lower left panel of Figure 1 does not have this problem.

To remedy the problem of large scatter shown in the "raw" light curves taken under the non-photometric condition, we employed a differential photometric technique (e.g., see Honeycutt 1992) to construct differential light curves for both the 10 s and 60 s data. In addition to the reduction of nightly data, the IPAC pipeline also created stacked reference images and the associated SExtractor reference catalogs (see Laher et al. 2014, for more details on how the reference images were created). We selected a subset of reference stars given in the SExtractor reference catalogs for the RR Lyrae listed in Table 1[14] to determine the mean magnitude differences, or relative zero-points Δm, between the reference stars and the nightly reduced catalogs. These reference stars have to meet with the following selection criteria: (1) exclude the targeted RR Lyrae stars in the reference catalogs; (2) $FLAGS = 0$ in the SExtractor catalog; (3) SExtractor parameter $CLASS\_STAR > 0.95$ (for stars-galaxies separation); (4) $15 < MAG\_AUTO < 17$ in the reference catalogs for the 60 s data (or $13 < MAG\_AUTO < 15$ for the 10 s data) such that stars with good enough signal-to-noise ratios were retained; and (5) more than 20 detections in nightly single-epoch catalogs (only for a few RR Lyrae stars, do the number of detections need to be tuned to a smaller value). For each of the RR Lyrae stars, we then loop over the nightly single-epoch catalogs and cross-matched to the corresponding reference stars using a 2 arc-second search radius. Furthermore, we removed reference stars that might be variables using the following procedure: (1) calculate the mean variance of the photometric errors based on the "raw" light curves, $\langle\sigma_m^2\rangle$; (2) calculate the variance of the "raw" light curves using the median absolute deviation (MAD) algorithm, σ_{LC}^2; and (3) remove stars with $|\sigma_{LC}^2 - \langle\sigma_m^2\rangle| > 0.1$. For the remaining reference stars (for each of the RR Lyrae), the Δm values are taken to be the median difference between the magnitudes from reference stars and the magnitudes in each single-epoch catalogs. The final adopted Δm were then applied to the "raw" light curves to construct the differential light curves. The middle panels of

[12] http://irsa.ipac.caltech.edu/applications/ptf/
[13] An example of such a script can be found at http://phares.caltech.edu/iptf/iptf_SummerSchool_2014/Miller2_problems.html.
[14] The only exception is for RR Lyrae KIC 3733346, because there are only 7 $R_{\rm PTF}$-band images taken with the PTF/iPTF observations. For this RR Lyrae, we selected the best seeing image and catalog as reference.

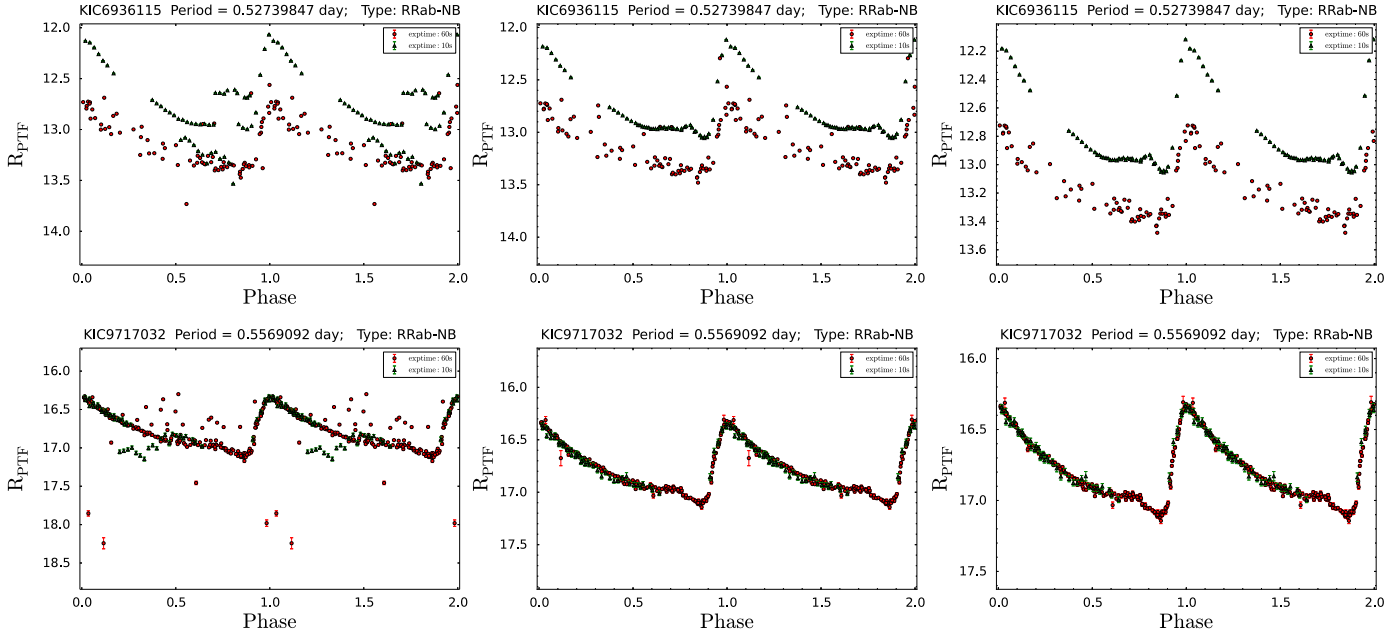

Figure 1. Left panel: example of extracted light curves for a bright RRab star (top panel) and a faint RRab star (bottom panel) from PTF/iPTF `SExtractor` catalogs without any further photometric refinement. Middle panel: refined light curves after applying the differential photometry technique as described in the text. Right panel: further refinement of light curves after removing obvious outlier(s) from the 60 s light curves and adding a small magnitude shift to the 10 s light curves. Red filled circles and green triangles are for data with 60 s exposure time (from regular PTF/iPTF surveys) and 10 s exposure time (from the dedicated iPTF experiment).

Figure 1 present the improvement of the light curves based on our procedures for the two example RR Lyrae.

Several RR Lyrae in our sample still displayed few obvious outliers in the refined differential light curves and/or small offsets between the 60 s and 10 s light curves (see the middle panels of Figure 1). Those outliers were manually removed, and a small magnitude offset (which is smaller than 0.05 mag) is added to the 10 s light curves if needed. The right panels of Figure 1 present the final refined light curves for the two exampled RR Lyrae. The final adopted differential light curves for the Blazhko and non-Blazhko RRab stars in our sample will be displayed in the next section. Note that the magnitudes in these light curves are not in absolute scale, as the a common zeropoint of $R_{\rm PTF} = 27.0$ was adopted when constructing the reference catalogs (Laher et al. 2014). Nevertheless, this would not affect the determination of Fourier parameters from these differential light curves, because Fourier parameters are independent of the global photometric calibration.

4.1. Excluded RRab Stars

We excluded the following RRab stars from our sample due to various reasons described below.

KIC 3733346: this bright RR Lyrae star only has seven data points in the $R_{\rm PTF}$-band light curve (see top panel of Figure 2) and hence does not permit a meaningful fitting of the Fourier parameter.

KIC 7198959: the prototype RR Lyr is too bright to be included in the 10 s observation, and the photometry (even after applying the differential light-curve technique) is severely affected by saturation. The light curve of this RR Lyrae is shown in the bottom panel of Figure 2.

KIC 4484128: this RR Lyrae is located within the footprint of CCD 03—the only CCD chip that is out of function at the beginning of PTF/iPTF surveys, and hence no data collected from the PTF and iPTF observations.

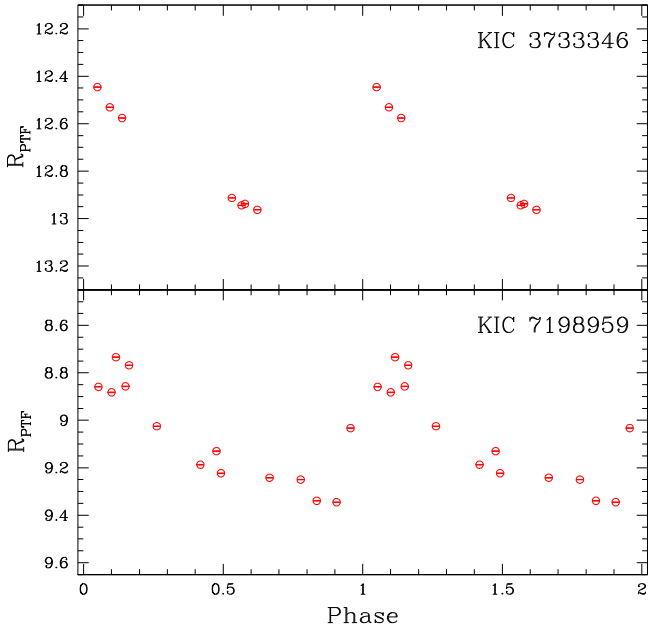

Figure 2. PTF 60 s $R_{\rm PTF}$-band light curves for two bright RR Lyrae: KIC 3733346 (top panel) and KIC 7198959 (the prototype RR Lyr itself, bottom panel). Both light curves were excluded in our analysis.

KIC 7021124: photometry of this RR Lyrae was affected by the diffraction spike from a nearby bright star and a very close star with similar brightness, as shown in the left panel of Figure 3. Therefore, we excluded this RR Lyrae in our sample. Differential light curves for this RR Lyrae were displayed in the right panel of Figure 3.

KIC 3864443 and *KIC 6186029*: based on the long-term and almost continuous observations from *Kepler*, Nemec et al. (2013) identified these two RR Lyrae as extreme Blazhko stars because they exhibit large amplitudes and phase modulations

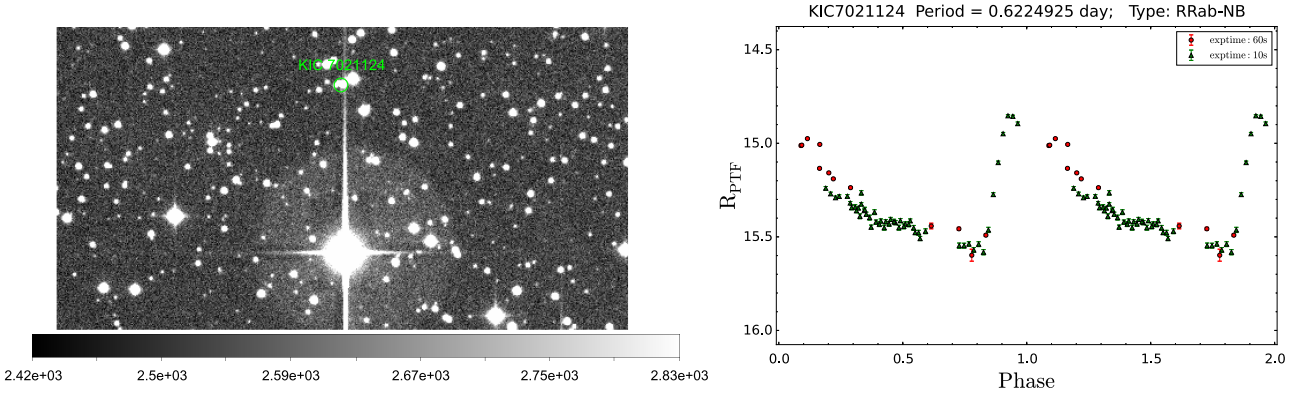

Figure 3. Left panel: a portion of the R_{PTF}-band image showing the influence of a diffraction spike from a nearby star on RR Lyrae KIC 7021124. Right panel: the 60 s (red circles) and 10 s (green triangles) differential light curves for this RR Lyrae.

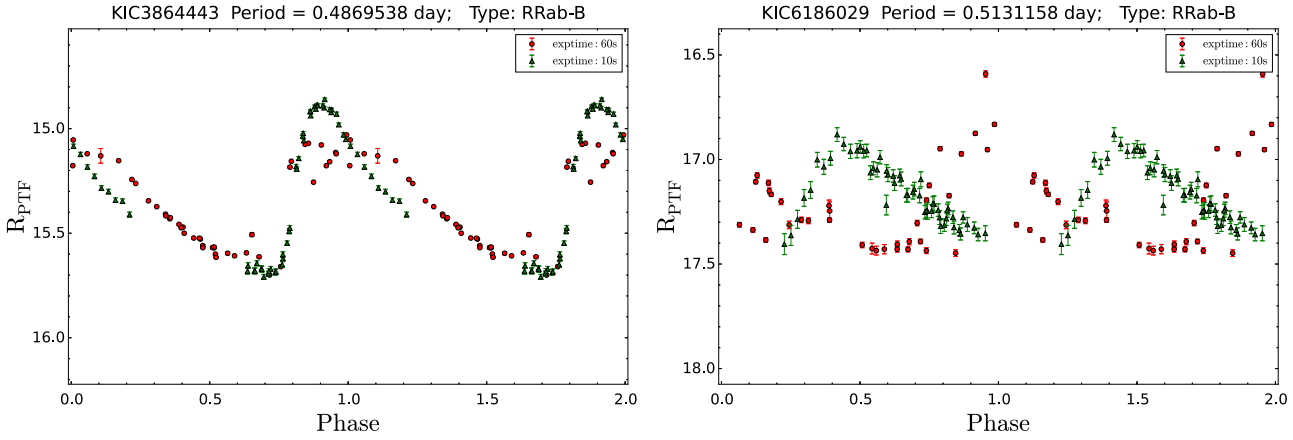

Figure 4. PTF R_{PTF}-band light curves for the two extreme Blazhko RR Lyrae identified in Nemec et al. (2013). The red circles and green triangles are for the 60 s and 10 s, respectively, differential light curves.

when compared to other Blazhko RR Lyrae in the *Kepler* field. Figure 4 shows their R_{PTF}-band light curves, which also displayed obvious Blazhko modulations. Note that Nemec et al. (2013) excluded them in their analysis; therefore, we also excluded them in our sample. Further analysis and discussion on KIC 6186029 (V445 Lyr) can be found in Guggenberger et al. (2012).

5. DERIVING THE ϕ_{31} FOURIER PARAMETERS

5.1. For Non-blazhko RRab Stars

Differential light curves for the remaining 19 non-Blazhko RR Lyrae stars were fitted with the truncated Fourier decomposition as given in Equation (1). We fit the 60 s and the 10 s light curves separately, as well as to the combined light curves. The best-fit orders n of the Fourier decomposition were chosen based on visual inspection of the fitted light curves. For the majority of the 10 s light curves, a relatively large gap was seen in the phased light curves, which affected the fitted light curves when applying the Fourier decomposition technique. To remedy this, we added a data point near the mid-point of the phased gap either taken from the 60 s light curves (for faint RR Lyrae) or derived from a cubic spline interpolation function (for bright RR Lyrae). Note that we only applied this additional data point to the 10 s light curves and not to the 60 s light curves. The only exception is the 10 s light curve for KIC 7176080, at which the phased gap is too large to apply a meaningful Fourier fit.

Among the 19 non-Blazhko RR Lyrae stars, three RR Lyrae do not have 10 s light curves and their 60 s light curves are displayed in Figure 5. The 60 s and 10 s phased light curves for the rest of the 16 non-Blazhko RR Lyrae were shown in the top and middle panels for each of the sub-figures in Figure 6. The dashed curves displayed in Figures 5 and 6 are the fitted light curves based on the Fourier decomposition technique. We compared the low-order Fourier parameters, R_{21}, R_{31}, ϕ_{21}, and ϕ_{31}, calculated with Equation (2), between the 60 s and 10 s light curves. The difference of the Fourier parameters as a function of mean R_{PTF}-band magnitudes is given in Figure 7. As can be seen from this figure, light curves with mean magnitudes fainter than ~14 mag show a smaller dispersion of the difference in Fourier parameters than those with mean magnitudes brighter than ~14 mag. Therefore, we merged the 60 s and 10 s light curves for the eight faint non-Blazhko RR Lyrae. For other eight bright non-Blazhko RR Lyrae, we added few data points from the 60 s light curves that have $FLAG = 0$ in the `SExtractor` catalogs, as these data points follow the light curve shapes defined by the 10 s light curves. We referred the merged 60 s and 10 s light curves as the combined light curves, as shown in bottom panels in each sub-figure of Figure 6. The final adopted ϕ_{31} Fourier parameters, based on these combined light curves, for the non-Blazhko RRab stars are listed in Table 3.

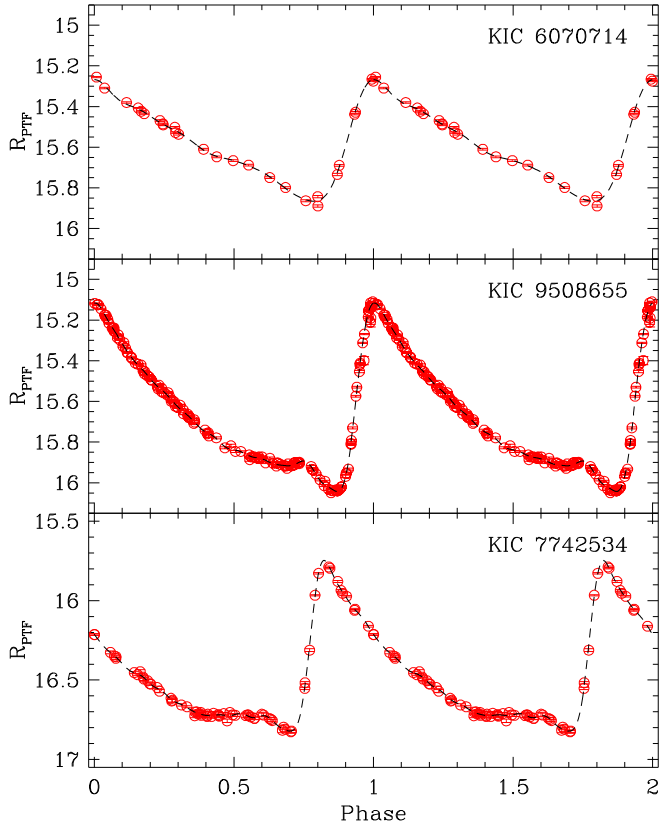

Figure 5. Differential light curves for three non-Blazhko RR Lyrae stars in our sample after applying the differential photometry technique as described in the text. These three RR Lyrae only have the 60 s observations. The dashed curves are the fitted light curves using Fourier expansion as given in Equation (1).

5.2. For Blazhko RRab Stars

For the remaining 12 Blazhko RRab stars in our sample, seven of them have both 10 s and 60 s light curves, and only KIC 11125706 has a mean magnitude brighter than ~14 mag. Therefore, we only fit the 10 s light curve of this star, and merged the 10 s and 60 s light curves for the other six Blazhko RRab stars. The differential light curves for these 12 Blazhko RRab stars were displayed in upper panels of Figure 8. Due to the amplitude and/or phase modulation, these light curves are "noisier" than the light curves of non-Blazhko RRab stars. Based on a similar approach presented in Smolec (2005), these modulated light curves were fitted with the following expression (for examples, see Kovács 1995; Alcock et al. 2003; Benkő et al. 2011):

$$m(t) = F_0(t, f_0) + F_m(t, f_0, f_m), \quad (3)$$

where F_0 is the same as in Equation (1):

$$F_0(t, f_0) = m_0 + \sum_{i=1}^{n} A_i \sin(2\pi i f_0 t + \phi_i),$$

and F_m includes the modulated components:

$$F_m(t, f_0, f_m) = \sum_{j=0}^{r} A_j^m \sin(2\pi j f_m t + \phi_j^m) + \sum_{k=0}^{q} A_k^- \sin[2\pi(k f_0 - f_m)t + \phi_k^-] + \sum_{k=0}^{q} A_k^+ \sin[2\pi(k f_0 + f_m)t + \phi_k^+].$$

In Equation (3), $f_0 = 1/P$ is the fundamental frequency, $f_m = 1/P_{BL}$ is the modulated frequency, and $A_0^m = A_0^- = A_0^+ = 0$. The Blazhko periods, P_{BL}, of these Blazhko RRab stars have already been derived in Nemec et al. (2013), and we adopted their values in this work.[15] Various combinations of Fourier order (n, r, q) were visually inspected, and the best-fit combinations were adopted. Following an approach similar to that of Smolec (2005), we removed the F_m components that are associated with the modulated frequency f_m after fitting the light curves with Equation (3). The resulted light curves were shown in lower panels of Figure 8, and were used to determine the ϕ_{31} Fourier parameters of these Blazhko RRab stars. Except for KIC 9973633, these light curves resemble the light curves for RR Lyrae stars pulsating in the fundamental frequency (and its harmonics) only.

The differential light curve for KIC 9973633 exhibits strong amplitude and phase modulation, similar to KIC 3864443 and KIC 6186029 (as shown in Figure 4). After experimenting with various combinations of Fourier order (n, r, q) to fit the combined 10 s and 60 s light curves with Equation (3), we still could not remove the modulated components in the combined light curve (see lower panel in Figure 8). This implies that additional frequency terms, such as $kf_0 \pm lf_m$ (where l is an integer), might need to be included in Equation (3), or this Blazhko star exhibits complex modulations as in the case of KIC 6186029 (V445 Lyr, Guggenberger et al. 2012). Nevertheless, a detailed investigation of the power spectrum of KIC 9973633 is beyond the scope of this work, and it is obvious that it should be excluded from our sample.

6. THE METALLICITY–LIGHT CURVE RELATION

The ϕ_{31} Fourier parameters derived in the previous section were listed in the third column of Table 3. Among these RRab stars, 26 of them have [Fe/H] values, listed in the forth column of Table 3, based on high-resolution spectroscopic observations taken from the 3.6 m Canada–France–Hawaii Telescope and the 10 m Keck I Telescope (Nemec et al. 2013). To derive the R_{PTF}-band metallicity–light curve relation, we adopted the well established regression function as in Jurcsik & Kovács (1996) and Wu et al. (2006): $[Fe/H] = b_0 + b_1 P + b_2 \phi_{31}$. We did not adopt the five-parameter regression function from Nemec et al. (2013) because it did not improve the dispersion (σ) of the fitted relation. The initial fit to the 26 RRab stars given in Table 3 returns a $\sigma \sim 0.20$ dex, which is much higher than the typical dispersion based on this technique (~0.13 dex to ~0.14 dex, Jurcsik & Kovács 1996; Wu et al. 2006; Ngeow 2015). After removing outliers that deviate more than 2×0.13 dex from the regression, we derived the following relation,[16] in the native R_{PTF}-band photometric system:

$$[Fe/H]_{PTF} = -4.089(\pm 0.339) - 7.346(\pm 0.439)P + 1.280(\pm 0.062)\phi_{31}, \quad (4)$$

with a dispersion of $\sigma = 0.118$ dex. Uncertainty on the photometric [Fe/H] based on the above equation, which

[15] There are two and three P_{BL} listed for KIC 9001926 and KIC 10789273, respectively. We adopted the first value given in Nemec et al. (2013) when fitting Equation (3) to their light curves.

[16] The actual regression fitting was done via the `kmpfit` package, available at https://github.com/josephmeiring/kmpfit, because errors are presented in both the independent variable ϕ_{31} and the dependent variable [Fe/H].

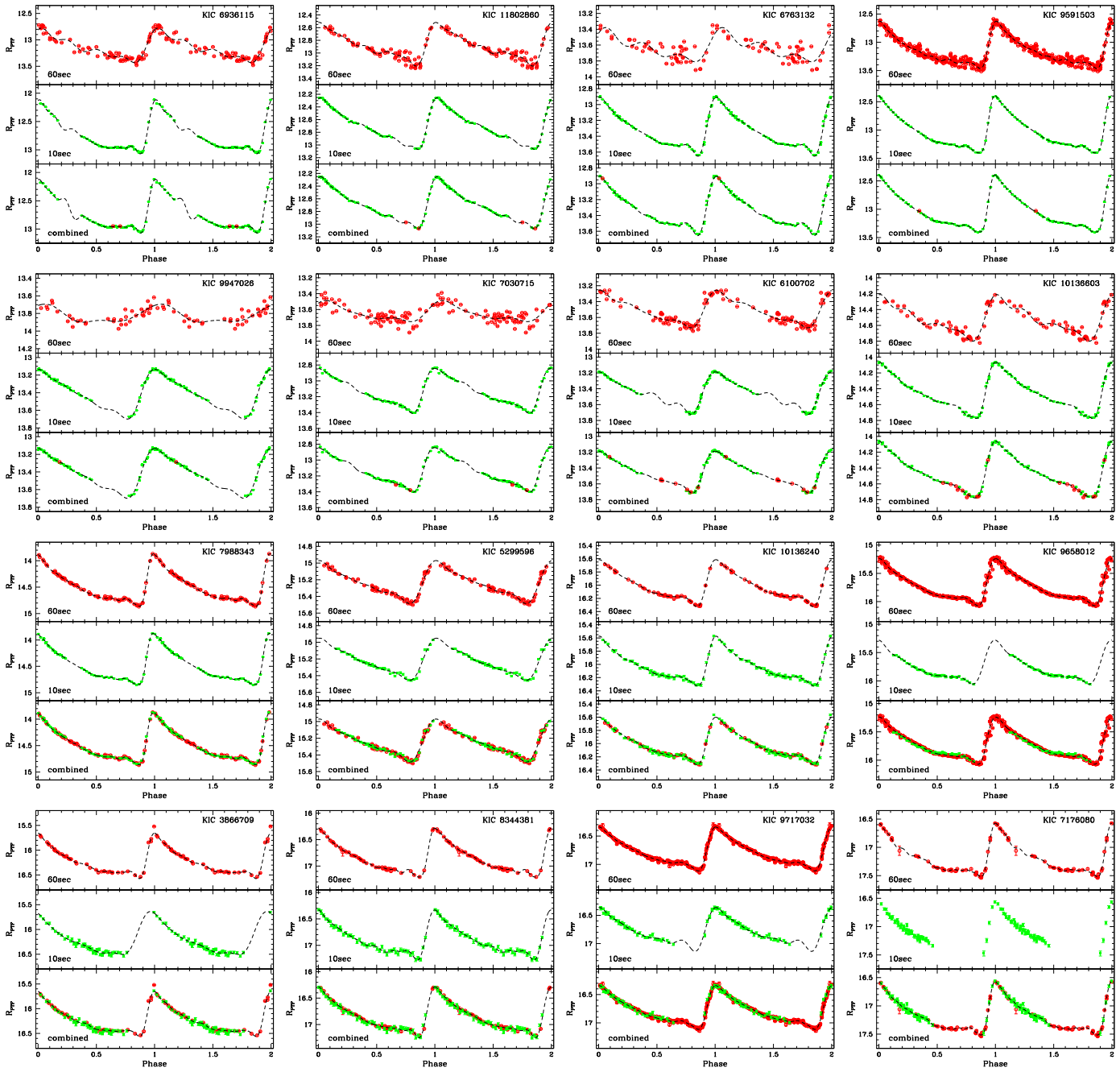

Figure 6. Differential light curves for non-Blazhko RR Lyrae stars in our sample after applying the differential photometry technique as described in the text. Red (opened) circles and green (filled) squares are for data with 60 s exposure times (from regular PTF/iPTF surveys, top panels in each sub-figure) and 10 s exposure times (from the dedicated iPTF experiment, middle panels in each sub-figure), respectively. Bottom panels in the sub-figures are the combined light curves (see the text for further details). The dashed curves are the fitted light curves using Fourier expansion as given in Equation (1).

incorporates the covariance matrix, can be calculated with the following expression.

$$\sigma^2_{[\mathrm{Fe/H}]} = 0.115 + 0.193P^2 + 0.004\phi^2_{31} - 0.103P - 0.031\phi_{31} - 0.020P\phi_{31} + 1.638\sigma^2_{\phi_{31}} + 53.965\sigma^2_P. \quad (5)$$

The fifth column in Table 3 listed the photometric [Fe/H] in the native R_{PTF}-band and the associated uncertainties calculated from Equation (4) and (5). Note that we assume $\sigma_P = 0$ for the RRab stars in the *Kepler* field as their very precise and accurate periods were determined from nearly continuous *Kepler* light curves (Nemec et al. 2013).

In Figure 9, we compare the photometric metallicities derived from Equation (4) to the spectroscopic metallicities given in Nemec et al. (2013). A clear outlier, KIC 11802860, can be seen from the top panel of this figure. We will discuss this outlier further in the next section. Figure 9(b) shows the difference between the photometric and spectroscopic metallicities (Δ) as a function of spectroscopic metallicity. Excluding KIC 11802860, these RRab stars have a $|\Delta|$ less than $\sim$0.35 dex (or 3σ, where $\sigma = 0.118$ is the dispersion of Equation (4)), with a mean Δ of -0.028 dex. Out of the 26

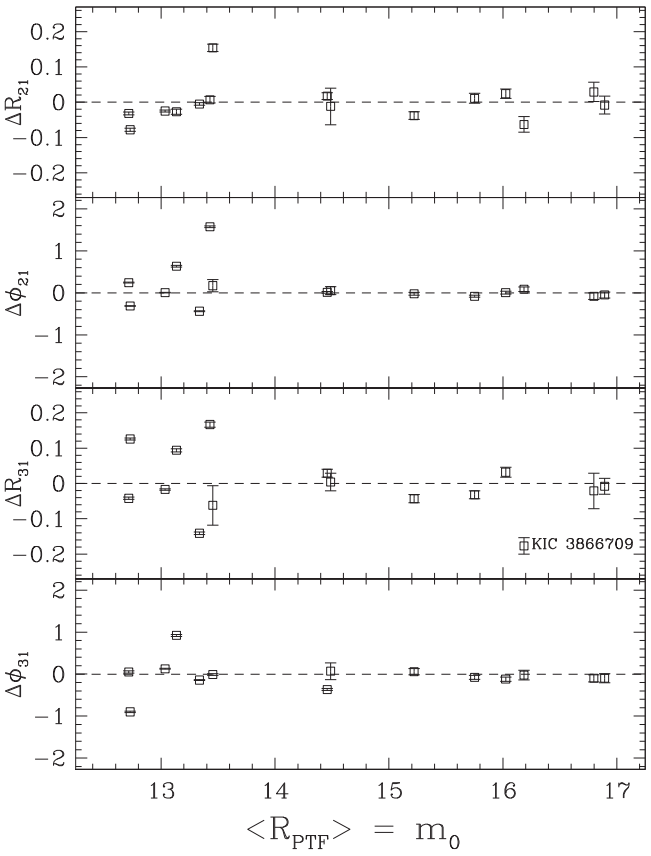

Figure 7. Difference, Δ, of the lower order Fourier parameters between the 60 s and 10 s light curves, where the Fourier parameters were calculated via Equation (2). The horizontal dashed lines indicate the cases of $\Delta = 0$, and not the fit to the data. The mean magnitude m_0 is calculated from the Fourier decomposition as given in Equation (1). The "outlier" in the ΔR_{31} plot is KIC 3866709, at which the fitting of Fourier decomposition to the 10 s light curves was affected by the phased gap at the ascendant branch.

RRab stars, 20 and 13 of them fall within the 2σ and 1σ boundaries, respectively. When comparing two quantities, it is customary in astronomy for these quantities to be considered in agreement if their absolute difference is within two to three times the quadrature sum of their errors. In Figure 9(c), we present the ratios of absolute difference of the two metallicities and their quadrature sum errors, at which the majority of them fall within the ratio of approximately three.

The Blazhko RRab stars in the *Kepler* field provide an opportunity to test the applicability of using their modulated light curves in estimating the ϕ_{31} Fourier parameter and hence the photometric metallicity. For the 11 Blazhko RRab stars in our *Kepler* sample (excluding KIC 9973633), we fit the light curves of the Blazhko RRab stars as presented in the upper panels of Figure 8 using Equation (1) only, without removing the modulated components (i.e., the F_m term as done in Section 5.2). For differential comparison, we adopted the same order n in the Fourier decomposition as in the case of including the modulated components. We found that several Blazhko RRab stars show a small difference in the ϕ_{31} Fourier parameter (KIC 9001926: 0.001; KIC 10789273: 0.013; KIC 12155928: 0.015) with and without removing the modulated components, while few others the differences are much larger (KIC 5559631: 0.233; KIC 11125706: 0.295; KIC 7671081: 0.666). The averaged difference of 0.102 translates to a difference of 0.13 dex in $[Fe/H]_{PTF}$ from Equation (4), which is comparable to the dispersion of the metallicity–light curve relation. Excluding KIC 7671081, the averaged difference in the ϕ_{31} Fourier parameter is reduced to 0.045 or a difference of 0.06 dex in $[Fe/H]_{PTF}$. Therefore, except for a few cases, our test suggested the Blazhko RRab stars can be included in the estimation of photometric $[Fe/H]_{PTF}$, given that their Blazhko periods can be well determined.

In the following sub-sections, we test and verify our metallicity–light curve relation using the new spectra data from a low-resolution spectroscopic observation of few RRab stars in the *Kepler* field (Section 6.1), as well as several publicly available data taken from the literature (Sections 6.2–6.3).

6.1. P200 Observations on Selected RR Lyrae in the Kepler Field

Spectra of several RRab stars listed in Table 3 were obtained with the P200 Telescope, using the available low-resolution spectrograph DBSP (the Double-Beam Spectrograph; Oke & Gunn 1982, with $R \sim 1360$), on 2015 June 20 and August 08. These spectra were reduced using a `pyRAF`-based reduction pipeline[17] tailored for the P200/DBSP spectrograph (Bellm & Sesar 2016; Bellm et al. 2016), including the bias subtraction, flat-field correction, spectral extraction, and wavelength calibration. Spectroscopic metallicity were then measured on these reduced spectra using the pseudo-equivalent widths of Balmer lines and [Ca II] K lines, following the procedures outlined in Sesar et al. (2012, hereafter S12) and Sesar et al. (2013, hereafter S13). To avoid line broadening due to velocity gradients and shock waves, Nemec et al. (2013) only took the spectra at pulsational phases between ~0.2 and ~0.5. Since only a small fraction of the P200/DBSP spectra fall within this range of pulsational phases, we adopted the criterion given in Sesar et al. (2013) to retain those spectra taken at the pulsational phases between 0.10 and 0.85 in order to increase usable P200/DBSP spectra in our sample. The six RRab stars and their measured metallicities from the P200/DBSP observations were listed in Table 4, and their spectra are presented in Figure 10. Two of the six RRab stars were observed on both nights. Also, three of the RRab stars have spectroscopic metallicities obtained from high-resolution spectra (Nemec et al. 2013), which can be used to compare to the spectroscopic metallicities taken from P200/DBSP.

Since the coefficients in the transformation of pseudo-equivalent widths were slightly different in S12 and S13, we measured the metallicity using both transformations. They are listed in columns 5 and 6 in Table 4 as $[Fe/H]_{S12}$ and $[Fe/H]_{S13}$, respectively. We assume an uncertainty of ~0.15 dex on these metallicities, which is a typical value based on the method of using pseudo-equivalent widths (Sesar et al. 2012). As shown in Table 4, the two prescriptions give consistent spectroscopic metallicities (except for KIC 10136603, with the largest difference of 0.29 dex), with $[Fe/H]_{S13}$ being more metal-poor than $[Fe/H]_{S12}$ by ~0.1 dex on average. When compared to the metallicity from high-resolution spectra ($[Fe/H]_{spec}$), excellent agreement was found for KIC 6763132 taken on August 08, followed by marginal agreements for KIC 9591503 and KIC 6763132 taken on June 20. For KIC 10136603, even though the values for both $[Fe/H]_{S12}$ and $[Fe/H]_{spec}$ indicate a metal-rich RRab star, they

[17] Available at https://github.com/ebellm/pyraf-dbsp.

Table 3
Fitted Results for Fourier Parameter ϕ_{31} from PTF Light Curves and the Derived Photometric Metallicity

KIC	P [days][a]	ϕ_{31}	$[Fe/H]_{spec}$[a]	$[Fe/H]_{PTF}$
		Non-Blazhko RR Lyrae		
6936115	0.52739847	4.796 ± 0.019	−1.98 ± 0.09	−1.82 ± 0.05
11802860	0.6872160	5.644 ± 0.007	−1.33 ± 0.09	−1.91 ± 0.07
6763132	0.5877887	5.207 ± 0.010	−1.89 ± 0.10	−1.74 ± 0.04
9591503	0.5713866	5.178 ± 0.012	−1.66 ± 0.12	−1.66 ± 0.04
9947026	0.5485905	5.946 ± 0.040	−0.59 ± 0.13	−0.51 ± 0.06
7030715	0.68361247	5.971 ± 0.023	−1.33 ± 0.08	−1.47 ± 0.07
6100702	0.4881457	5.803 ± 0.017	−0.16 ± 0.09	−0.25 ± 0.05
10136603	0.4337747	5.764 ± 0.013	−0.05 ± 0.14	0.10 ± 0.07
7988343	0.5811436	5.130 ± 0.005	⋯	−1.79 ± 0.04
6070714	0.5340941	6.210 ± 0.029	−0.05 ± 0.10	−0.06 ± 0.07
5299596	0.5236377	5.949 ± 0.016	−0.42 ± 0.10	−0.32 ± 0.05
10136240	0.5657781	5.406 ± 0.019	−1.29 ± 0.23	−1.33 ± 0.04
9508655	0.5942369	5.215 ± 0.008	−1.83 ± 0.12	−1.78 ± 0.04
9658012	0.533206	5.250 ± 0.006	−1.28 ± 0.14	−1.29 ± 0.03
7742534	0.4564851	4.886 ± 0.028	−1.28 ± 0.20	−1.19 ± 0.06
3866709	0.47070609	4.876 ± 0.033	−1.13 ± 0.09	−1.31 ± 0.06
8344381	0.5768288	5.260 ± 0.033	⋯	−1.59 ± 0.05
9717032	0.5569092	5.340 ± 0.016	−1.27 ± 0.15	−1.35 ± 0.04
7176080	0.5070740	4.954 ± 0.039	⋯	−1.47 ± 0.06
		Blazhko RR Lyrae		
11125706	0.6132200	6.098 ± 0.021	−1.09 ± 0.08	−0.79 ± 0.05
10789273	0.48027971	5.068 ± 0.015	−1.01 ± 0.10	−1.13 ± 0.04
7505345	0.4737027	5.027 ± 0.005	−1.14 ± 0.17	−1.13 ± 0.04
5559631	0.62070001	5.967 ± 0.011	−1.16 ± 0.11	−1.01 ± 0.05
12155928	0.43638507	4.983 ± 0.005	−1.23 ± 0.15	−0.92 ± 0.05
9697825	0.5575765	4.947 ± 0.016	−1.50 ± 0.29	−1.85 ± 0.05
6183128	0.561691	5.137 ± 0.019	−1.44 ± 0.16	−1.64 ± 0.04
9578833	0.5270283	5.069 ± 0.043	−1.16 ± 0.09	−1.47 ± 0.07
7257008	0.51177516	5.163 ± 0.051	⋯	−1.24 ± 0.07
7671081	0.5046123	5.134 ± 0.050	−1.51 ± 0.12	−1.22 ± 0.07
9001926	0.5568016	5.220 ± 0.020	−1.50 ± 0.20	−1.50 ± 0.04

Note.
[a] Values are taken from Nemec et al. (2013).

are not in agreement with each others. In contrast, the value from $[Fe/H]_{S13}$ is closer to $[Fe/H]_{spec}$ for this RRab star. In short, values from $[Fe/H]_{S13}$ are in better agreement with those from $[Fe/H]_{spec}$ than those from $[Fe/H]_{S12}$, with a mean difference of ∼0.25 dex and ∼0.38 dex, respectively.

When comparing the metallicities from P200/DBSP spectra to photometric metallicities based on PTF/iPTF light curves ($[Fe/H]_{PTF}$), we found that good agreements can be seen in three RRab stars: KIC 6763132, KIC 9591503, and KIC 8344381. Based on the five measurements of low-resolution spectroscopic metallicities for these three RRab stars, the $[Fe/H]_{S13}$ values are again in better agreement with $[Fe/H]_{PTF}$ than those from $[Fe/H]_{S12}$, the mean difference becomes ∼0.05 dex and ∼0.14 dex, respectively. For KIC 10136603, $[Fe/H]_{S12}$ disagrees with $[Fe/H]_{PTF}$ and yet $[Fe/H]_{S13}$ marginally agrees with the latter value. Finally, both KIC 7176080 and KIC 7257008 show large discrepancies between the metallicities from P200/DBSP spectra and PTF/iPTF light curves, by more than 1.5 dex. We suspected that this might be caused by noisier spectra toward the short-wavelength ends. Figure 11 compares the transformed pseudo-equivalent widths for the eight spectra, those from KIC 7176080, KIC 7257008, and KIC 10136603 appeared to be outliers in this figure. Another possibility is that the observations of KIC 7176080 and KIC 7257008 were affected by weather because their spectra were taken within 10 minutes of each other on June 20. A similar result and conclusion can also be found when comparing $[Fe/H]_{S12/S13}$ to $[Fe/H]_{Kp}$.

For the two RRab stars, KIC 6763132 and KIC 8344381, that have two P200/DBSP observations, the arithmetic average of the $[Fe/H]_{S12/S13}$ values are listed in the last two rows of Table 4. These averaged values were in good agreement with those from $[Fe/H]_{PTF}$, in particular, excellent agreements can be seen between the values of $[Fe/H]_{S13}$ and $[Fe/H]_{PTF}$. Note that the difference of the measured spectroscopic metallicities at the two different pulsation phases is ∼±0.35 dex for these two RRab stars.

6.2. RR Lyrae Samples in K2E2 Field

Molnár et al. (2015) presented the light-curve analysis for 27 RRab stars toward Pisces. These light-curve data were taken under the K2 Two-wheel Engineering Test (hereafter K2E2) after the failure of the second reaction wheel on board *Kepler*. Based on the 8.9-day light curves, Molnár et al. (2015) classified 13 of them as non-Blazhko RRab stars, and the

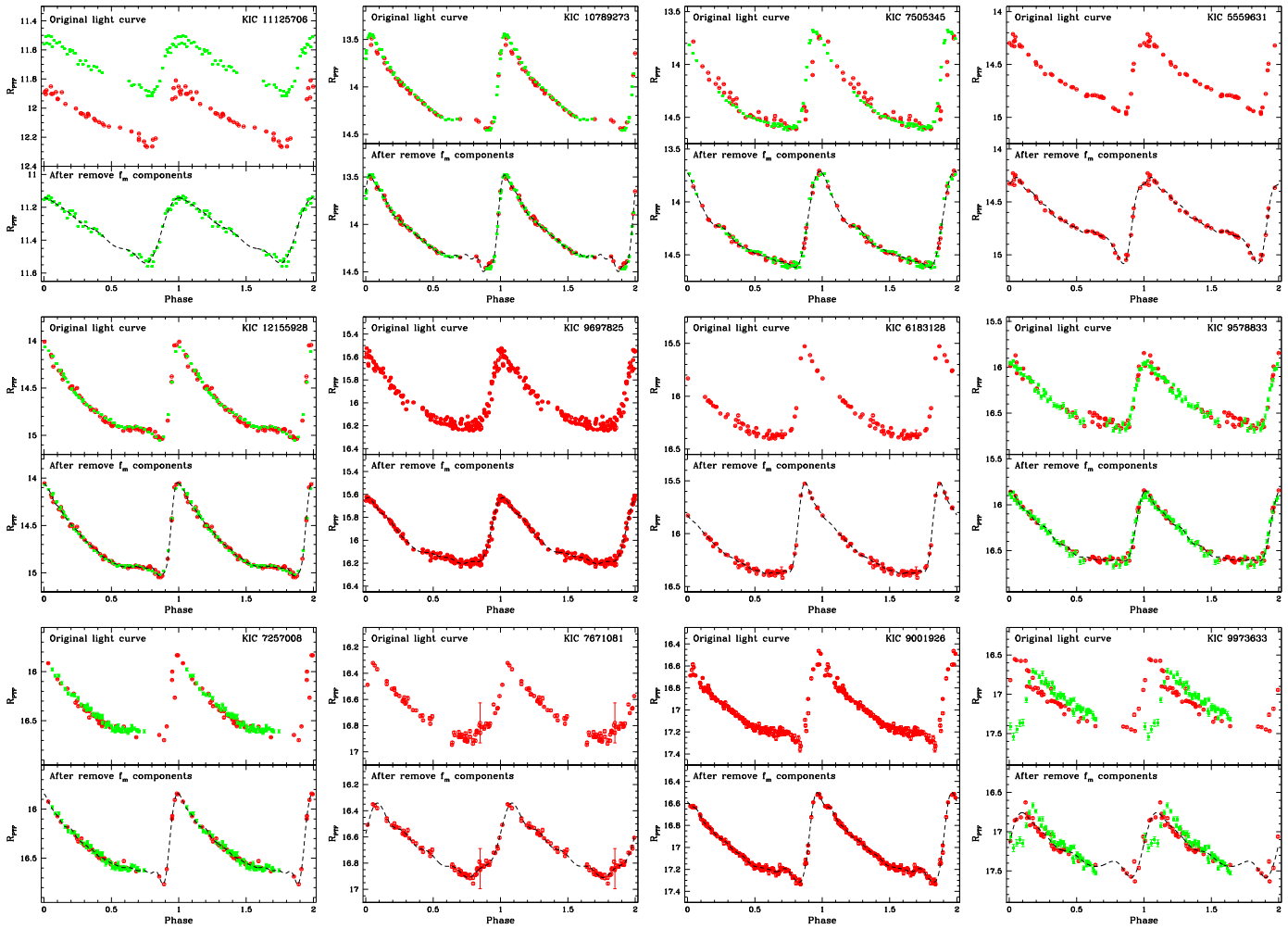

Figure 8. Upper panels of each of the sub-figures display the "original" differential light curves for Blazhko RR Lyrae stars in our sample after applying the differential photometry technique as described in the text. Bottom panels of each of the sub-figures are the light curves after removing the components related to the modulated (Blazhko) frequencies f_m, and the dashed curves are the fitted light curves using Fourier expansion as given in Equation (1). Red filled circles and green triangles are for data with 60 s exposure times (from regular PTF/iPTF surveys) and 10 s exposure times (from the dedicated iPTF experiment).

remaining 14 of them are Blazhko RRab stars.[18] These authors also derived the photometric metallicity $[Fe/H]_{Kp}$ based on the K2E2 light curves with the relation presented in Nemec et al. (2013). Therefore, the RRab stars in the K2E2 Field provide a sizable sample to test our metallicity–light curve relation. We retrieved and constructed the PTF light curves for 24 of these RRab stars using the same approaches as described in Section 4, the remaining three (EPIC 60018663, 60018669, and 60018779) either fell on the inoperational CCD 03 or on the gap between the CCD chips. Number of data points per light curves for these RRab star ranges from ∼30 to ∼240. Similar to Section 5, these light curves were fitted with Equation (1) to determine the Fourier parameters ϕ_{31} and hence the photometric metallicity $[Fe/H]_{PTF}$ with Equation (4). We did not remove the F_m components for the Blazhko RRab stars because the majority of them do not have modulated period determined in Molnár et al. (2015). Nevertheless, this also provides an opportunity to test our metallicity–light curve relation in the absence of modulated period. Finally, pulsation periods are taken from Molnár et al. (2015), and assume that $\sigma_P \sim 0$.

Similar to Figure 9, we compare the photometric metallicities for these RRab stars based on PTF light curves and K2K2 light curves in Figure 12. After removing the two clear outliers shown in Figure 12(a), the remaining 22 RRab stars show a mean Δ of -0.093 dex, which is consistent with the accuracy of this technique (Kovács 2005). Separating the sample into non-Blazhko RRab stars and Blazhko RRab stars, we obtained a mean Δ of -0.094 dex and -0.092 dex, respectively, suggesting that similar results can be achieved without removing the modulated component for Blazhko RRab stars. Besides the two outliers, there are only two other RRab stars with $|\Delta| > 0.35$ dex. For the remaining 22 RRab stars, there are 15 and 8 located within the 2σ and 1σ boundaries, respectively, as shown in Figure 12(b). Similarly, Figure 12(c) demonstrates that all of the RRab stars have a $|\Delta|/\sigma_T < 3$, except for the two extreme outliers. Our test suggested that Equation (4) can be used to provide reliable metallicity estimation for the majority of RRab stars. Figure 13 displays three examples of the R_{PTF}-band light curves with the

[18] Even though three of them are possible modulated RRab stars, for simplicity, we grouped them into the Blazhko RRab stars.

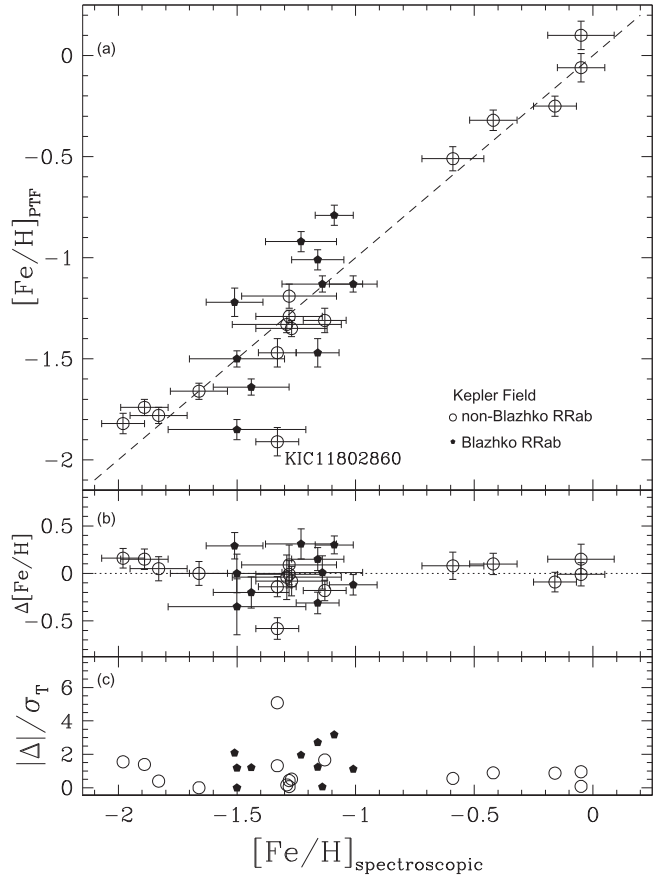

Figure 9. (a): Comparison of the photometric [Fe/H], calculated from Equation (4), in native $R_{\rm PTF}$-band to the spectroscopic [Fe/H] as presented in Nemec et al. (2013) for the common 26 RRab stars in the *Kepler* field. The dashed line indicates $y = x$ and not the fit to the data. A clear outlier, KIC 11802860, is also marked in the plot. (b): Difference between the photometric and spectroscopic [Fe/H] as a function of spectroscopic metallicity. The dotted lines are for $\Delta = 0$ and not the fit to the data. (c): Ratio of the absolute difference and σ_T as a function of spectroscopic metallicity, where σ_T is the quadrature sum of the uncertainties of photometric and spectroscopic metallicities. Open and filled symbols represent the non-Blazhko and Blazhko RRab stars, respectively.

best (right panel) and the worst (left panel) agreements of the photometric metallicities, respectively.

6.3. RR Lyrae Samples from Sesar et al. (2012, 2013)

As part of the study to search for substructures and tidal streams in the Galactic halo, S12 and S13 searched for the distant RRab stars using the PTF and other survey data. S12 reported the finding of 10 RR Lyrae with spectroscopic follow-up observations using two low-resolution spectrographs, the P200/DBSP and the Low Resolution Imaging Spectrometer (LRIS; Oke et al. 1995, with $R \sim 1760$, equipped on the Keck I Telescope). S13 presented 94 RRab stars of which only 50 of them have spectroscopic observations with P200/DBSP. Spectroscopic metallicities of these RRab stars were then measured from the low-resolution spectra. We retrieved PTF/iPTF light curves for the majority of these RRab stars and fit with Equation (1) following the procedures described in Sections 4 and 5. Pulsation periods of these RRab stars were adopted from S12 and S13.

Since 2012, more data have become available from the iPTF project for the 10 RRab stars listed in S12. The number of data points per light curve increased from merely ∼1% (from 271 to ∼290 for S12_RR6) to ∼180% (from 82 to ∼235 for S12_RR9) as compared to S12, with a range from ∼190 to ∼660. Besides a larger number of data points, these 10 RRab stars are also much fainter than those found in the K2E2 Field shown in the previous subsection, with mean magnitudes fainter than ∼19.5 mag. Consequently, their light curves exhibit a much larger scatter than the K2E2 RRab stars, as displayed in Figure 14. Nevertheless, these RRab stars provide an opportunity to test our metallicity–light curve relation for the faint RRab stars. Comparison of the photometric metallicities and spectroscopic metallicities of the nine RRab stars shown in Figure 14 are given in Figure 15 as filled symbols. The mean Δ of these nine RRab stars is 0.31 dex, after removing the three outliers in Figure 15 this mean value drops to 0.24 dex. Five of the six remaining faint RRab stars have a $|\Delta|$ value less than the 3σ (i.e., ∼0.35 dex) boundary. Hence, the performance of our metallicity–light curve relation is

Table 4
Metallicity for Selected RRab Stars in the *Kepler* Field with P200/DBSP Observations

KIC	Type[a]	Observed Date	Exposure time[b]	$[Fe/H]_{S12}$	$[Fe/H]_{S13}$	$[Fe/H]_{spec}$[c]	$[Fe/H]_{Kp}$[c]	$[Fe/H]_{PTF}$
6763132	RRab-NB	2015 Jun 20	240	−1.48	−1.54	−1.89 ± 0.10	−1.81 ± 0.03	−1.74 ± 0.04
6763132	RRab-NB	2015 Aug 08	300	−1.83	−1.90	−1.89 ± 0.10	−1.81 ± 0.03	−1.74 ± 0.04
9591503	RRab-NB	2015 Aug 08	300	−1.39	−1.48	−1.66 ± 0.12	−1.74 ± 0.03	−1.66 ± 0.04
10136603	RRab-NB	2015 Aug 08	300	0.72	0.43	−0.05 ± 0.14	−0.06 ± 0.05	0.10 ± 0.07
7176080	RRab-NB	2015 Jun 20	300	0.37	0.15	⋯	−1.63 ± 0.04	−1.47 ± 0.06
8344381	RRab-NB	2015 Jun 20	300	−1.65	−1.75	⋯	−1.82 ± 0.03	−1.59 ± 0.05
8344381	RRab-NB	2015 Aug 08	300	−1.28	−1.40	⋯	−1.82 ± 0.03	−1.59 ± 0.05
7257008	RRab-B	2015 Jun 20	300	0.29	0.31	⋯	−1.02 ± 0.03	−1.24 ± 0.07
Averaged $[Fe/H]_{S12}$ and $[Fe/H]_{S13}$ values for KIC 6763132 and KIC 8344381								
6763132	RRab-NB	⋯	⋯	−1.66	−1.72	−1.89 ± 0.10	−1.81 ± 0.03	−1.74 ± 0.04
8344381	RRab-NB	⋯	⋯	−1.47	−1.58	⋯	−1.82 ± 0.03	−1.59 ± 0.05

Notes.
[a] Types are the same as in Table 1.
[b] Exposure time in seconds for the P200/DBSP observations.
[c] Adopted from Nemec et al. (2013).

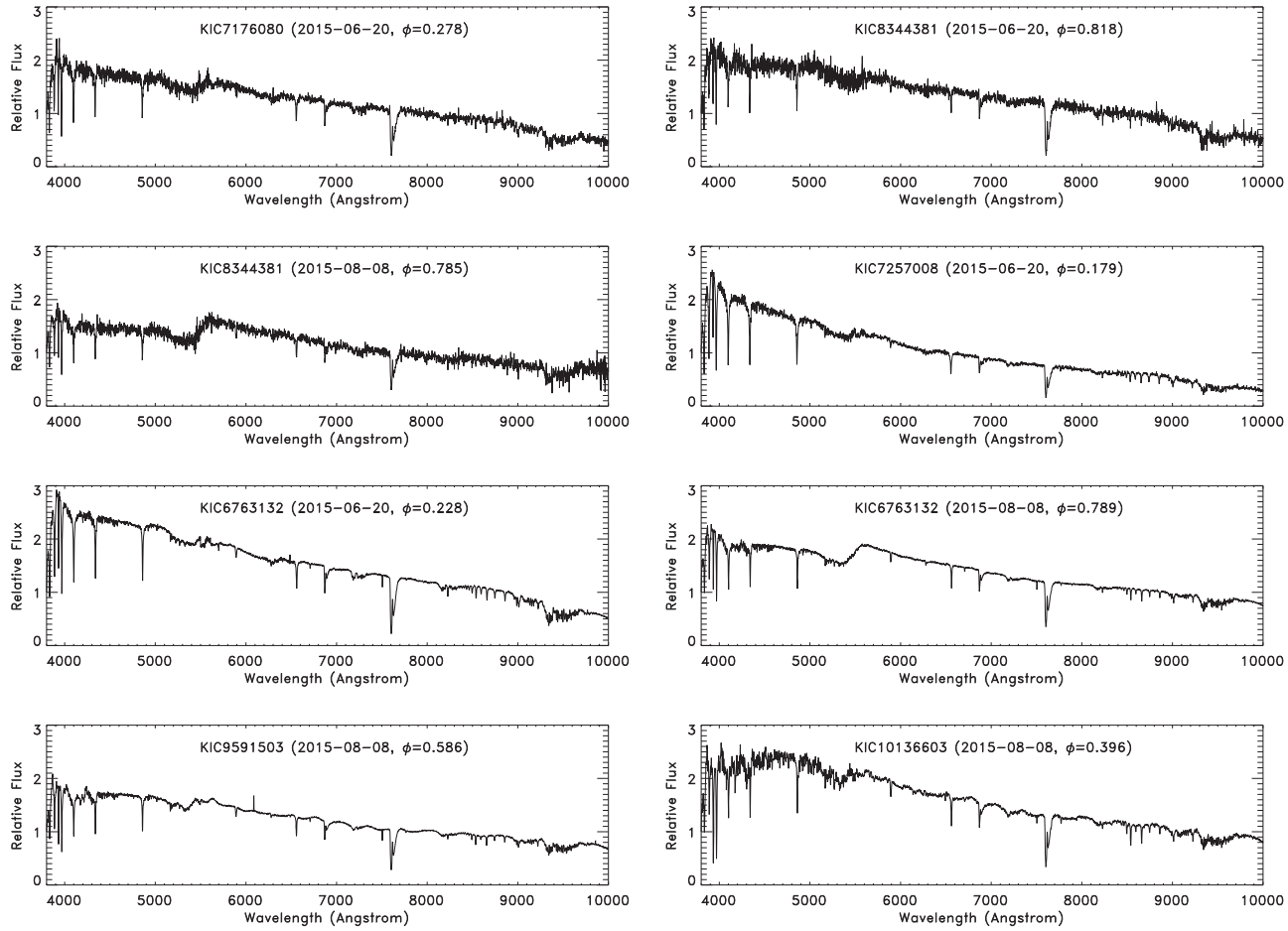

Figure 10. P200/DBSP low-resolution spectra for the RRab stars listed in Table 4. Flux is normalized to the flux at 3800 Å of each target. ϕ represents the pulsation phases when the spectra were taken.

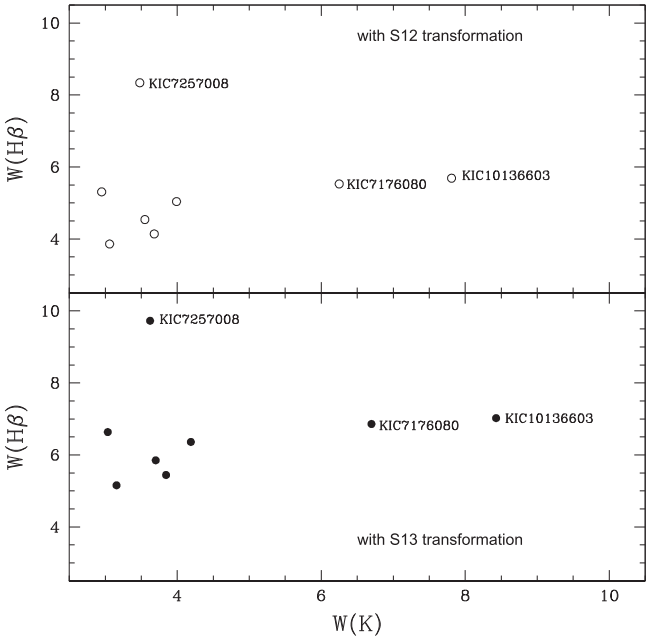

Figure 11. Comparison of the transformed pseudo-equivalent widths for [Ca II] K lines and $H\beta$ lines from the eight spectra taken from P200/DBSP observations (see Table 4), with transformations given in S12 (upper panel) and S13 (lower panel).

acceptable given the faintness, large scatter of light curves, and small number of RRab stars in this sample.

For the 50 RRab stars in S13, we only retained the PTF/iPTF light curves for 32 of them, the rest of the RRab stars either do not have data in PTF/iPTF (i.e., fall into the CCD 03), with only a small number of data points per light curve (less than 15 data points), or the light curves do not exhibit RRab-like light curves. The number of data points for these 32 RRab stars include ∼20 to ∼70 for 26 of them, ∼100 to ∼300 for 5 of them, and ∼580 for 1 of them. These RRab stars are brighter than those in S12, with mean magnitudes ranging from ∼17 mag. to ∼19 mag. Figure 15 compares the photometric and spectroscopic metallicities for these 32 RRab stars as open symbols, which exhibit a much larger scatter than the RRab stars in the K2E2 Fields (Figure 12). Without removing any outliers, the mean value of Δ for this sample is 0.23 dex.

Figure 16 presents $R_{\rm PTF}$-band light curves for the selected RRab stars in this sample. Left panels of Figure 16 display examples of three light curves that give a good agreement between the photometric and spectroscopic metallicities. In contrast, the middle panels of Figure 16 show the light curves of three RRab stars with the largest Δ, ranging from 0.84 dex (for S13_RR6) to 1.31 dex (for S13_RR23). However, these light curves do not show any "abnormality" when compared to those on the left panels. The upper-right panel of Figure 16 is

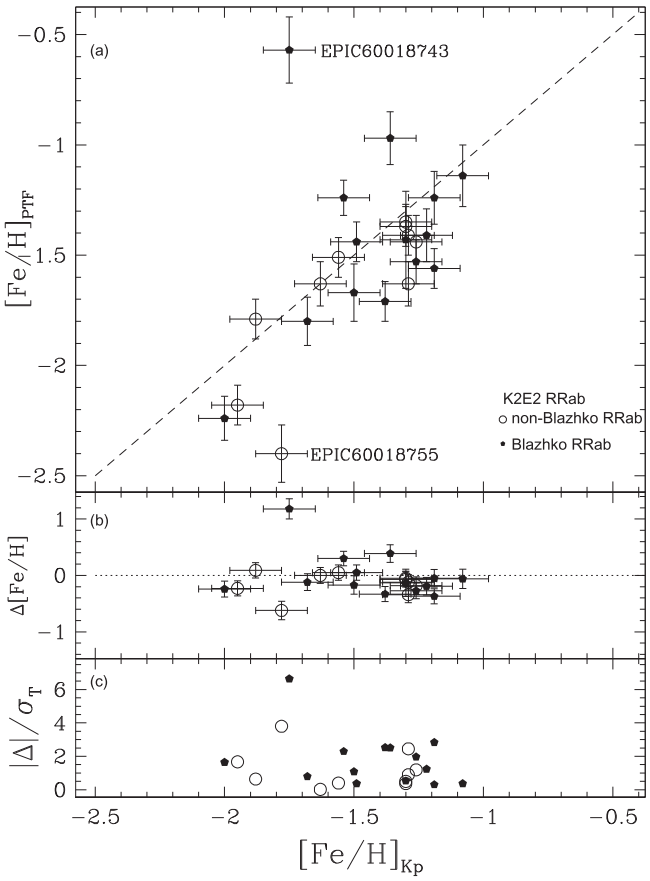

Figure 12. Same as in Figure 9, but for RRab stars in the K2E2 Field. Two obvious outliers are labeled in the plot. We adopted ±0.1 dex for the uncertainties on $[Fe/H]_{Kp}$ (Molnár et al. 2015).

the light curve for the only RRab star with ∼580 data points in this sample, which also display a large scatter as those in the S12 sample (see Figure 14). The middle-right panel of Figure 16 is the light curve for the most metal-poor RRab star within the 50 RR Lyrae in S13 sample, with a measured spectroscopic metallicity of −2.73 dex. We obtained a $[Fe/H]_{PTF} = -3.22 \pm 0.64$ dex that is consistent with the spectroscopic metallicity. Finally, the lower-right panel of Figure 16 shows the light curve of an RRab star with the largest $|\Delta|/\sigma_T$ ratio. The errors on metallicities for this RRab star are ∼0.15 dex, hence $\sigma_T \sim 0.21$ dex. However, this RRab star has a Δ of ∼0.79 dex, and a resulting a large value of $|\Delta|/\sigma_T$ ratio. After removing the five outliers (three in the middle panel of Figure 16, and the two in middle-right and lower-right panel of Figure 16), the mean Δ reduces to ∼0.15 dex for this sample, which is comparable to the accuracy of both methods.

7. DISCUSSION AND CONCLUSION

In this work, we derived the metallicity–light curve relation in the native R_{PTF}-band photometric system using the RRab stars found in the *Kepler* field. The main reasons for selecting this sample of RRab stars include the availability of accurate pulsation periods (based on *Kepler* light curves) and spectroscopic metallicities derived from high-resolution spectra (Nemec et al. 2013). Since about half of the RRab stars in the *Kepler* field are brighter than the saturation limit of $R_{PTF} \sim 14$ mag, we re-observed a number of them with a 10 s exposure time from a dedicated iPTF experiment. Our derived metallicity–light curve relation is presented in Equation (4). When we tested our metallicity–light curve relation for six RRab stars in the *Kepler* field with low-resolution P200/DBSP observations, we obtained mixed results with good agreements and discrepancies. The later cases might be due to problems in observed spectra rather than our relation. We further tested our relation with three samples taken from the literature and obtained overall good agreements with our derived [Fe/H] to the published values. Specifically, after removing outliers, we obtained the mean difference between our photometric metallicities and published metallicities with the following values: ∼−0.09 dex for the K2E2 RRab stars, ∼0.15 dex for the halo RRab stars in S13, and ∼0.24 dex for a few faint RRab stars in S12 (mainly due to the large scatters of the light curves). When we applied our relation to the only RRab star in the Boötes 3 dSphs galaxy, we derived $[Fe/H]_{PTF} = -2.15 \pm 0.28$ dex, which is consistent with the spectroscopic measurement given in Sesar et al. (2014, −2.0 ± 0.1 dex).

As a demonstration of the applicability of our metallicity–light curve relation, we derived the photometric metallicities for the RRab stars listed in Table 2 of Sesar et al. (2013) that did not have spectroscopic observations. Out of the 44 RRab stars listed in that table, we could only retrieved the PTF/iPTF light curves for 33 of them (for the same reasons as those mentioned in Section 6.3). The distribution of $[Fe/H]_{PTF}$ for this sample is similar to the 32 RRab stars taken from Table 1 of Sesar et al. (2013, for which their photometric metallicities have already been derived in Section 6.3), as demonstrated in Figure 17. In the near future, we can use our relation to select RR Lyrae candidates in the Galactic halo found from the Zwicky Transient Facility (ZTF, Bellm 2014; Smith et al. 2014) before requesting spectroscopic observations with large aperture telescopes for confirmation.[19] The ZTF project is using the same P48 Telescope and almost the same *R*-band filter as the PTF/iPTF projects, but with an upgraded mosaic CCD camera that fills out the focal plane of the P48 Telescope. With much improved survey rates, ZTF can accumulate a much larger number of data points per light curves for the RR Lyrae candidates, and their ϕ_{31} Fourier parameters and hence the photometric metallicity can be better constrained.

Figure 18 presents the low-order Fourier parameters for all of the RRab stars that have PTF/iPTF light curves and have been studied in this work. This figure also includes those outliers, shown in black symbols, when comparing the derived $[Fe/H]_{PTF}$ to published metallicities (see Section 6). In terms of Fourier parameters, these outliers are mostly confined within the parameter space defined by other RRab stars. Therefore, these outliers do not exhibit abnormality in terms of the PTF/iPTF light curves. We note that in previous studies, outliers were seen in the comparison of metallicities from (low-resolution) spectroscopic measurements and from the metallicity–light curve relation (see, for example, Kovács 2005; Wu et al. 2006). The causes of the majority of the outliers can be traced back to various reasons, including, stars exhibiting Blazhko modulation (without removing the modulated components), problems in the photometry and/or light curves (e.g., noisy light curves, gaps in phased light curves, issues due to

[19] For example, a faint RR Lyrae could be either a distant halo star or a highly extinct field star. If the derived photometric metallicity indicates a metal-poor RR Lyrae, then it is most likely a halo star and is worth the spectroscopic follow-up observations, and vice versa.

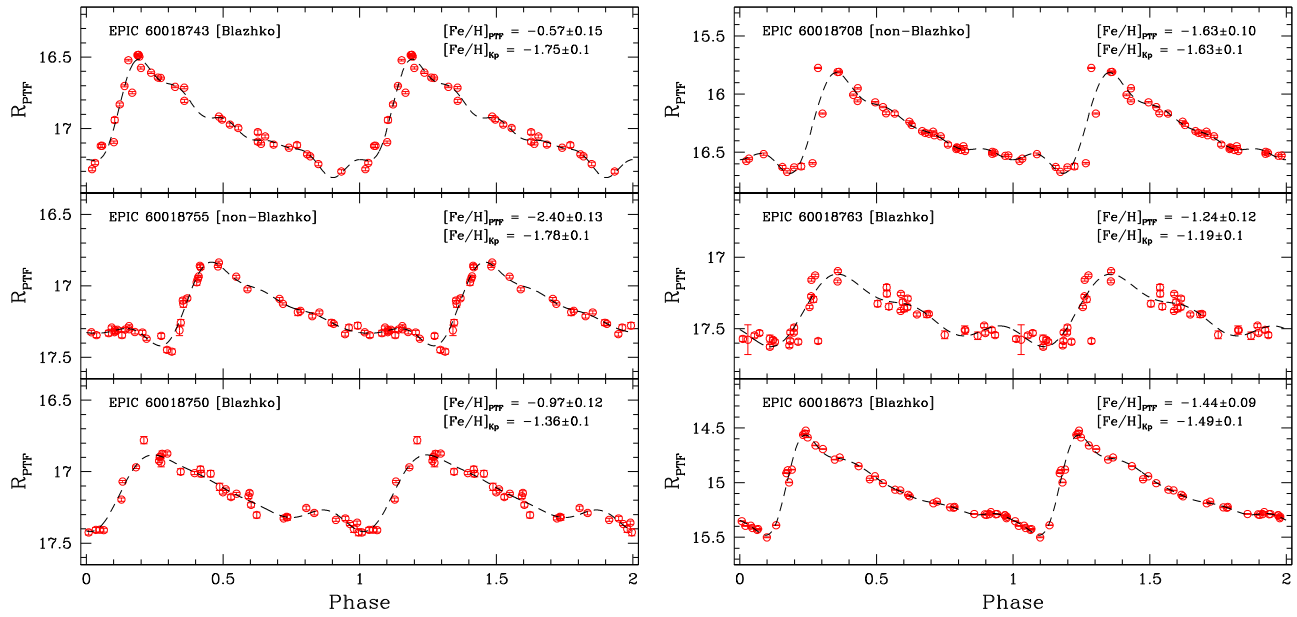

Figure 13. $R_{\rm PTF}$-band light curves for RRab stars in K2E2 Field that display the largest (left panels) and smallest (right panels) deviation of the derived photometric metallicities. Dashed curves are the best-fit light curves using Equation (1).

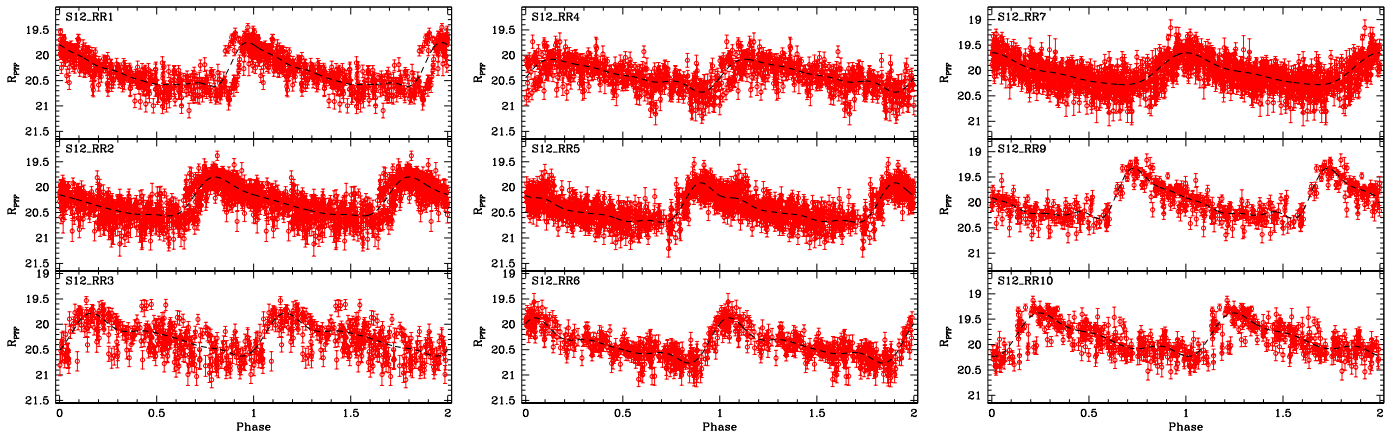

Figure 14. $R_{\rm PTF}$-band light curves for nine faint RRab stars taken from Sesar et al. (2012). The dashed curves are fitted light curves using Equation (1). We excluded S12_RR8 because its PTF/iPTF light curve (with 192 data points) is too scattered that it does not display a typical RRab-like light curve, in contrast to those presented in this figure.

photometric calibrations, etc.), inaccurate spectroscopic metallicity, or even the wrong pulsational period being adopted. However, there still exist few outliers that cannot be explained, for example, V341 Aql and DG Hya in Kovács (2005) and V341 Aql, UY Boo, DG Hya, RZ Cam, and BK And in Wu et al. (2006). In the following, we briefly discuss the possible causes of the 11 outliers marked in Figure 18. A detailed investigation of them is beyond the scope of this work.

KIC 11802860: this RRab star in the *Kepler* field is not a Blazhko variable, and its PTF/iPTF light curve did not show any obvious peculiarities. We do not believe the spectroscopic measurements are inaccurate because they were obtained with CFHT and this RRab star is quite bright (∼13 mag). We note that the ϕ_{31} Fourier parameter in Johnson-Cousin *R*-band derived from other dense ground-based observations is 5.639 for this RRab star (Jeon et al. 2014), which is in good agreement with the value listed in Table 3 (5.644 ± 0.007). Hence, there are no obvious reasons to explain why this RRab star appears to be an outlier.

EPIC 60018743 and EPIC 60018755: one of these RRab stars is a Blazhko variable (EPIC 60018743), and we did not remove its modulated component as in other Blazhko variables in the *Kepler* field (see Section 6.2). This might explain why this RRab star is an outlier. We do not think the photometric metallicities $[{\rm Fe/H}]_{Kp}$ are inaccurate because those measurements are based on almost continuous *Kepler* light curves. Nevertheless, the quality of the PTF/iPTF light curves for both of them are similar to other RRab stars in the same sample, as demonstrated in left and right panels of Figure 13. Their Fourier parameters also agree with other RRab stars at a similar period. The relatively small number of data points per light curve, ∼40 for both of them, might incorrectly estimate the ϕ_{31}

Fourier parameters. In the near future, the accumulation of a large number of data points from ZTF could assist in resolving the outlier status of these two RRab stars.

S12_RR2, S12_RR3, and S12_RR4: as shown in Figure 14, PTF/iPTF light curves for these three RRab stars, as well as others in the same sample, are noisy because they are faint RRab stars and hence their photometric measurements are less accurate. This could partially explain why these three RRab stars are outliers. However, their Fourier parameters also agree with other RRab stars, except S12_RR3 in ϕ_{21} plot (upper-left panel in Figure 18). Sesar et al. (2012) noted that the spectroscopic metallicities for S12_RR3 were differed by 0.5 dex from two measurements with different instruments. In contrast, the other two RRab stars (S12_RR1 and S12_RR5) with three spectroscopic observations show very good agreement of measured metallicity (within 0.2 dex). The low-resolution spectroscopic observation could also partially contribute to the outlier status of these three RRab stars, especially for S12_RR2 and S12_RR4 at which they only have one measurement taken from P200/DBSP. Our observations

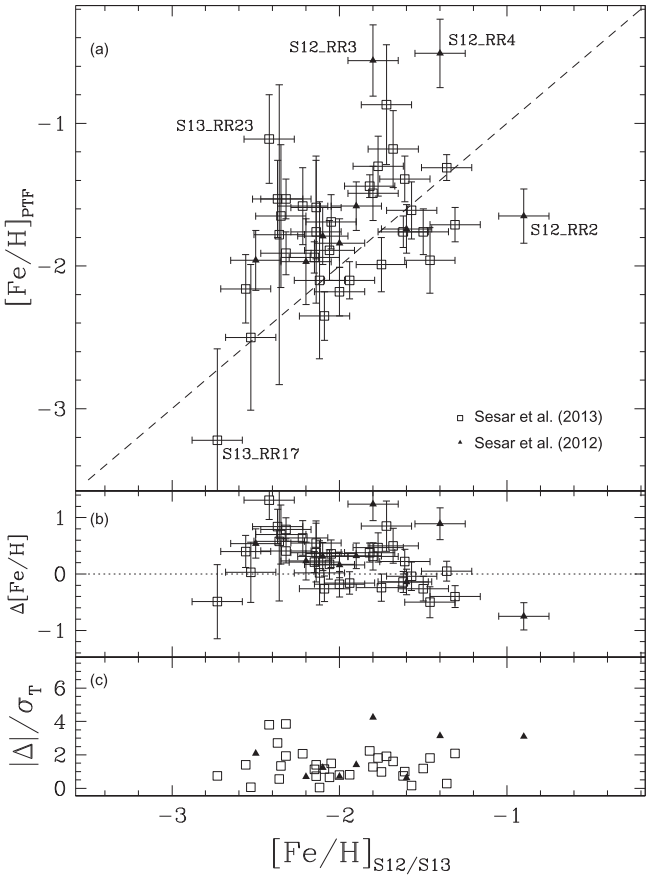

Figure 15. Same as in Figure 9, but for RRab stars taken from Sesar et al. (2012) and Sesar et al. (2013). Five obvious outliers are labeled in the plot. We adopted ±0.15 dex for the uncertainties on $[Fe/H]_{S12/S13}$ (Sesar et al. 2012), where $S12/S13$ represents the metallicity measured from low-resolution spectra (Sesar et al. 2012, 2013). We took an arithmetic mean if an RRab star has more than one spectroscopic metallicities listed in Sesar et al. (2012).

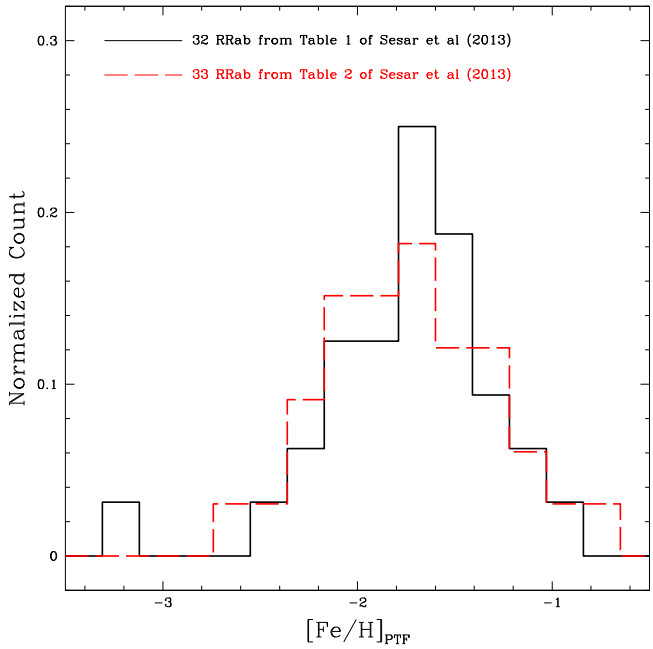

Figure 17. Distributions of the photometric metallicities based on available PTF/iPTF light curves for RRab stars in Tables 1 and 2 from Sesar et al. (2013).

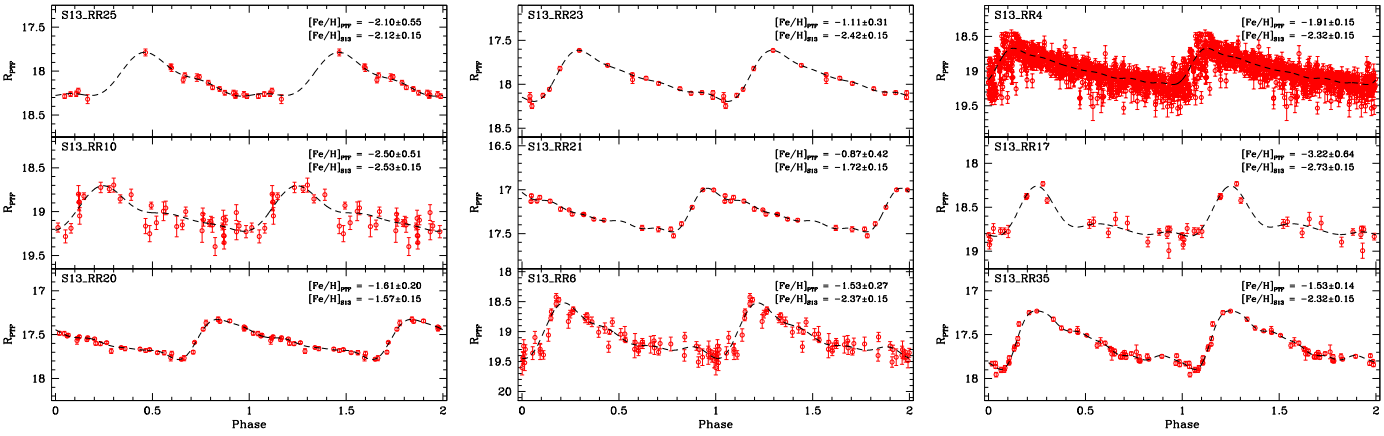

Figure 16. Left panel: example R_{PTF}-band light curves for three RRab stars with the smallest deviation between photometric and spectroscopic metallicities. Middle panel: example R_{PTF}-band light curves for three RRab stars with the largest deviation between photometric and spectroscopic metallicities. Right panel: example R_{PTF}-band light curves for three "unusual" RRab stars. The upper-right panel shows the light curve for the only RRab star with ∼580 data points in its light curve. The middle-right panel shows the light curve for the RRab star that has a $[Fe/H]_{PTF} < -3$ dex. The lower-right panel shows the light curve for the RRab star with the largest ratio of absolute difference of metallicities and the quadrature sum errors, $|\Delta|/\sigma_T \sim 3.85$, in the sample. The dashed curves are fitted light curves using Equation (1).

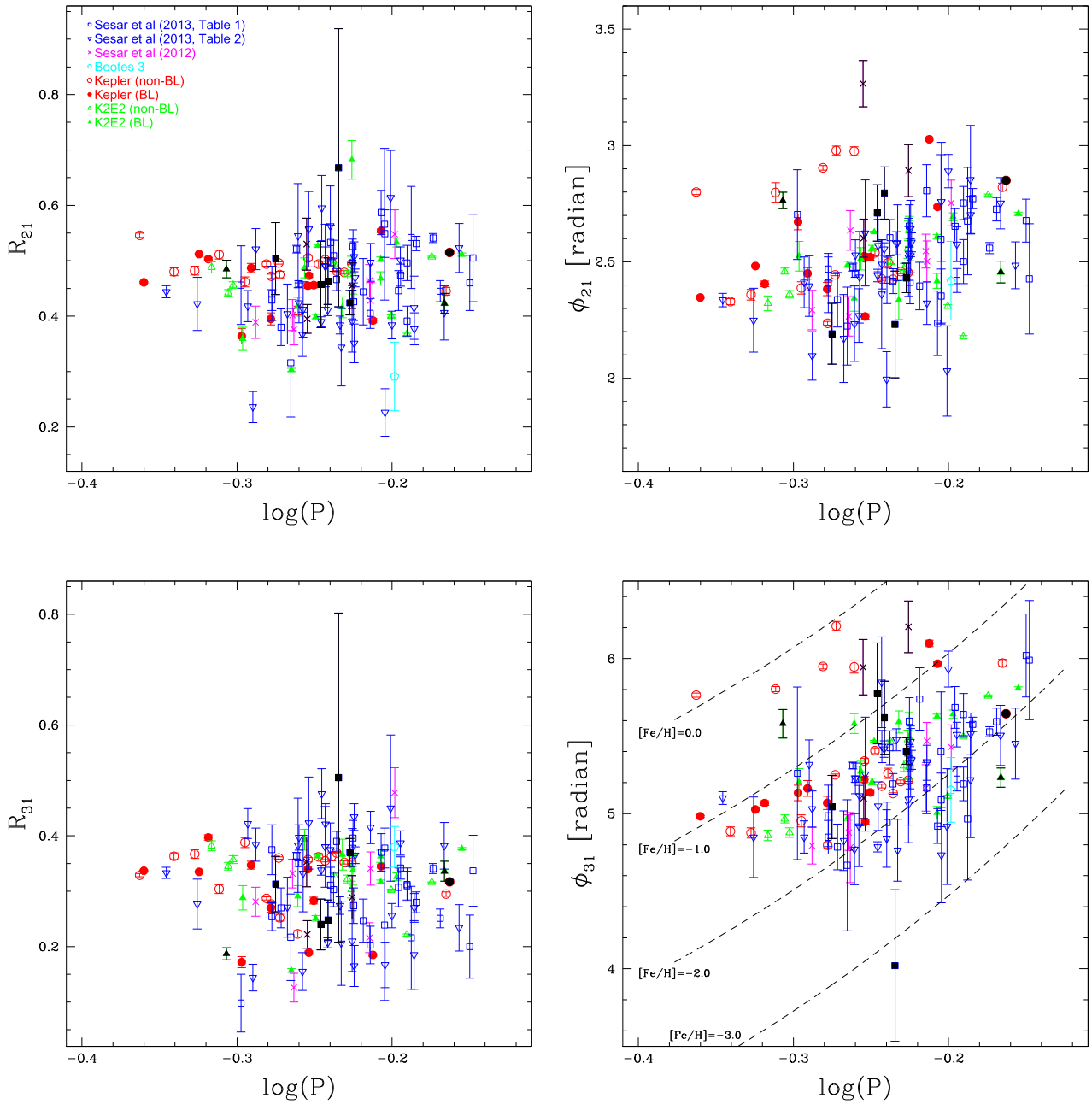

Figure 18. Low-order Fourier parameters, as defined in Equation (2), as a function of periods for all of the 129 RRab stars considered in this work. The different colored symbols represent various samples: red circles are for the RRab stars in the *Kepler* field, separated by filled symbols for Blazhko (BL) stars and opened symbols for non-Blazhko (non-BL) stars; upward triangles are for RRab stars from K2E2 Fields (again separated by Blazhko and non-Blazhko stars); crosses are for RR Lyrae taken from Sesar et al. (2012); squares and downward triangles are those from Tables 1 and 2 of Sesar et al. (2013), respectively. The filled symbols in black are the 11 rejected outliers as mentioned in Section 6. The filled squares in black with large errors bar are for S13_RR17. The black cross in the upper-left panel with $\phi_{21} \sim 3.3$ is for S12_RR3. The dashed curves in lower-right panel, for the ϕ_{31} Fourier parameters, show the expected ϕ_{31} at four different metallicities. These curves are constructed by inverting Equation (4).

with P200/DBSP, presented in Section 6.1, demonstrated that sometimes the P200/DBSP spectra could lead to an inaccurate measurement of metallicity. Finally, we pointed out that Kovács (2005) declared a spectroscopic metallicity is inaccurate if the number of measurements is less than three.

S13_RR6, S13_RR21, S13_RR23, and S13_RR35: Fourier parameters for these four RRab stars are located within the parameter space defined by all other RRab stars, as shown in Figure 18. Their PTF/iPTF light curves (see Figure 16) also did not exhibit any abnormality, except for S13_RR6, which is noisier. We therefore believe their ϕ_{31} values are reasonably estimated. Nevertheless, with additional accumulated data points per light curves from the ZTF, the accuracy of ϕ_{31} values, and hence their photometric metallicities, could be improved. As discussed previously, the possibility of inaccurate spectroscopic metallicity based on single observations from P200/DBSP could not be ruled out either.

S13_RR17: this RRab star has the largest errors on R_{21} and R_{31} Four parameters, and the second largest errors on ϕ_{21} and ϕ_{31} Four parameters. Its phased PTF/iPTF light curve also has a gap around the phase of ∼0.4. Furthermore, the minimum light for these RRab stars is near $R_{\rm PTF} \sim 19$ mag, hence the

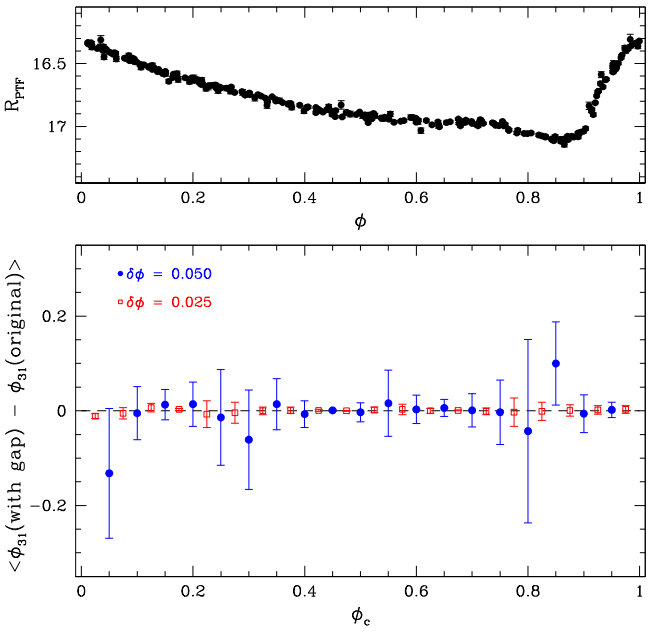

Figure 19. Results on testing the effect of phase gaps in observed light curves on the determination of the ϕ_{31} Fourier parameter, and hence the $[Fe/H]_{PTF}$ metallicity. The upper panel displays an example of a well-sampled light curve for a typical non-Blazhko RRab star, with maximum light located at phase zero ($\phi = 0$). The lower panel shows the weighted mean variations of ϕ_{31} (i.e., the difference of ϕ_{31} in the original light curves and after including a phase gap in the light curves) as a function of ϕ_c, the location of a phase gap that is artificially included in the phased light curves. The phase gap is created by removing those data points with ϕ falling within $\phi_c \pm \delta\phi$ of the well-sampled light curves. Open squares and filled circles shown in the lower panel are for the cases of $\delta\phi = 0.025$ (for a phase gap with a width of 0.05) and $\delta\phi = 0.050$ (for a phase gap with a width of 0.1), respectively. Error bars represent the standard deviations on the weighted means, based on the combined light curves for non-Blazhko RRab stars in the *Kepler* field that have large numbers of data points ($N > 120$, to ensure a good coverage of the light curve) in their light curves. The same Fourier order n was adopted in both of the original light curves and the light curves with artificial phase gap included. The dashed line indicates $y = 0$ and not the fit to the data points.

photometric measurements are less accurate around phases of minimum light. Combining these reasons, we believe the problems on the light curve lead to the inaccurate measurement of photometric metallicity, which is hence displayed as an outlier in Figure 15. This most metal-poor RRab star worth the collection of additional light curve data in the era of ZTF.

Finally, we examined the influence of a gap in phased light curves when determining the ϕ_{31} Fourier parameters, which translate to $[Fe/H]_{PTF}$ via Equation (4). We took several of the well-sampled light curves from the non-Blazhko RRab stars in the *Kepler* field and artificially removed some data points to mimic a phase gap in the light curves. Figure 19 presents the test results for the phase gap, with a width of 0.05 and 0.1, located at different parts of the phased light curve. In the case of a phase gap that has a width of 0.05, Figure 19 reveals that such a phase gap will not alter the determination of the ϕ_{31} Fourier parameters, regardless of the location of the phase gap. When the width of the phase gap is increased to 0.1, the ϕ_{31} Fourier parameters could be affected by the presence of the phase gap near the maximum or minimum light, as is indicated by the the two most deviated (filled circle) points in Figure 19. This result reiterates the finding in Wu et al. (2006), who suggested that the photometric metallicity can still be estimated from light curves with insufficient phase coverage when there are data points around the maximum or minimum light. In other phases around the ascending and descending branch of the light curve, the phase gap with width of 0.1 does not greatly affect the determination of the ϕ_{31} Fourier parameters. Certainly, the ϕ_{31} Fourier parameters would be less accurate when the width of the phase gap increases, and auxiliary techniques such as adding an interpolated data point in the gap (as employed in this work) or applying a polynomial fit (Jurcsik & Kovács 1996) are needed to recover the ϕ_{31} Fourier parameters. We anticipate that the problem of the phase gap presented in light curves will be diminished within the ZTF project because a much larger number of data points per light curve will be collected in the era of ZTF.

We thank the referee for valuable input that improved the manuscript. We acknowledge Wee Siang Edmund Yuen, a 2015 summer student at the National Central University, for carrying out the preliminary analysis of the PTF data for RR Lyrae in the *Kepler* field. C.C.N. is thankful for the funding from the Ministry of Science and Technology (Taiwan) under grants 104-2112-M-008-012-MY3 and 104-2119-M-008-024. This research has made use of the NASA/IPAC Infrared Science Archive, which is operated by the Jet Propulsion Laboratory, California Institute of Technology, under contract with the National Aeronautics and Space Administration.

Facility: PO:1.2m.

REFERENCES

Alcock, C., Alves, D. R., Becker, A., et al. 2003, ApJ, 598, 597
Bellm, E. C., Kaplan, D. L., Breton, R. P., et al. 2016, ApJ, 816, 74
Bellm, E. C., & Sesar, B. 2016, pyraf-dbsp: Reduction pipeline for the Palomar Double Beam Spectrograph, Astrophysics Source Code Library, ascl:1602.002
Bellm, E. 2014, in The Third Hot-wiring the Transient Universe Workshop, ed. P. R. Wozniak et al., 27
Benkő, J. M., Szabó, R., & Paparó, M. 2011, MNRAS, 417, 974
Bertin, E., & Arnouts, S. 1996, A&AS, 117, 393
Braga, V. F., Dall'Ora, M., Bono, G., et al. 2015, ApJ, 799, 165
Caputo, F., Castellani, V., Marconi, M., & Ripepi, V. 2000, MNRAS, 316, 819
Chang, C.-K., Ip, W.-H., Lin, H.-W., et al. 2014, ApJ, 788, 17
De Lee, N. 2008, PhD thesis, Michigan State Univ.
Deb, S., & Singh, H. P. 2009, A&A, 507, 1729
Deb, S., & Singh, H. P. 2010, MNRAS, 402, 691
Demarque, P., Zinn, R., Lee, Y.-W., & Yi, S. 2000, AJ, 119, 1398
Gratton, R. G., Bragaglia, A., Clementini, G., et al. 2004, A&A, 421, 937
Guggenberger, E., Kolenberg, K., Nemec, J. M., et al. 2012, MNRAS, 424, 649
Honeycutt, R. K. 1992, PASP, 104, 435
Jeon, Y.-B., Ngeow, C.-C., & Nemec, J. M. 2014, in Proc. IAU Symp. 301, Precision Asteroseismology, ed. J. A. Guzik et al. (Cambridge: Cambridge Univ. Press), 427
Jurcsik, J. 2003, A&A, 403, 587
Jurcsik, J., & Kovács, G. 1996, A&A, 312, 111
Kovács, G. 1995, A&A, 295, 693
Kovács, G. 2005, A&A, 438, 227
Kovács, G., & Zsoldos, E. 1995, A&A, 293, L57
Kunder, A., & Chaboyer, B. 2008, AJ, 136, 2441
Laher, R. R., Surace, J., Grillmair, C. J., et al. 2014, PASP, 126, 674
Law, N. M., Kulkarni, S. R., Dekany, R. G., et al. 2009, PASP, 121, 1395
Marconi, M., Coppola, G., Bono, G., et al. 2015, ApJ, 808, 50
Martinez-Vazquez, C. E., Monelli, M., Bono, G., et al. 2016, in Communications of the Konkoly Observatory Hungary 105 (Budapest: Konkoly Observatory), 53
McNamara, D. H. 1999, PASP, 111, 489
Molnár, L., Szabó, R., Moskalik, P. A., et al. 2015, MNRAS, 452, 4283
Nemec, J. M., Cohen, J. G., Ripepi, V., et al. 2013, ApJ, 773, 181
Nemec, J. M., Smolec, R., Benkő, J. M., et al. 2011, MNRAS, 417, 1022
Ngeow, C. C. 2015, in Proc. 2015 IEEE Int. Conf. on Space Science and Communication, ed. M. Singh et al., 302
Ofek, E. O., Laher, R., Law, N., et al. 2012a, PASP, 124, 62

Ofek, E. O., Laher, R., Surace, J., et al. 2012b, PASP, 124, 854
Oke, J. B., Cohen, J. G., Carr, M., et al. 1995, PASP, 107, 375
Oke, J. B., & Gunn, J. E. 1982, PASP, 94, 586
Oluseyi, H. M., Becker, A. C., Culliton, C., et al. 2012, AJ, 144, 9
Rahmer, G., Smith, R., Velur, V., et al. 2008, Proc. SPIE, 7014, 70144Y
Rau, A., Kulkarni, S. R., Law, N. M., et al. 2009, PASP, 121, 1334
Sandage, A. 2004, AJ, 128, 858
Sandage, A., & Tammann, G. A. 2006, ARA&A, 44, 93
Sesar, B., Banholzer, S. R., Cohen, J. G., et al. 2014, ApJ, 793, 135
Sesar, B., Cohen, J. G., Levitan, D., et al. 2012, ApJ, 755, 134
Sesar, B., Ivezić, Ž., Grammer, S. H., et al. 2010, ApJ, 708, 717
Sesar, B., Grillmair, C. J., Cohen, J. G., et al. 2013, ApJ, 776, 26
Simon, N. R. 1988, ApJ, 328, 747
Simon, N. R., & Lee, A. S. 1981, ApJ, 248, 291
Skowron, D. M., Soszyński, I., Udalski, A., et al. 2016, AcA, 66, 269
Smith, R. M., Dekany, R. G., Bebek, C., et al. 2014, Proc. SPIE, 9147, 914779
Smolec, R. 2005, AcA, 55, 59
Surace, J., Laher, R., Masci, F., Grillmair, C., & Helou, G. 2015, adass XXIV, 495, 197
van Eyken, J. C., Ciardi, D. R., Rebull, L. M., et al. 2011, AJ, 142, 60
Watkins, L. L., Evans, N. W., Belokurov, V., et al. 2009, MNRAS, 398, 1757
Wu, C., Qiu, Y. L., Deng, J. S., Hu, J. Y., & Zhao, Y. H. 2006, A&A, 453, 895